HHS Public Access

Author manuscript

Neurobiol Aging. Author manuscript; available in PMC 2022 September 01.

Published in final edited form as:

Neurobiol Aging. 2022 September ; 117: 44–58. doi:10.1016/j.neurobiolaging.2022.04.014.

Advanced age has dissociable effects on hippocampal CA1 ripples and CA3 high frequency events in male rats

Nicholas M. DiCola[a], **Alexa L. Lacy**[a], **Omar J. Bishr**[a], **Kathryn M. Kimsey**[a], **Jenna L. Whitney**[a], **Sarah D. Lovett**[a], **Sara N. Burke**[a,#,*], **Andrew P. Maurer**[a,b,c,#,**]

[a]Evelyn F. McKnight McKnight Brain Institute, Department of Neuroscience, University of Florida, Gainesville, FL, USA

[b]Department of Biomedical Engineering, University of Florida, Gainesville, FL, USA

[c]Engineering School of Sustainable Infrastructure and Environment, University of Florida, Gainesville, FL, USA

Abstract

Sharp wave/ripples/high frequency events (HFEs) are transient bursts of depolarization in hippocampal subregions CA3 and CA1 that occur during rest and pauses in behavior. Previous studies have reported that CA1 ripples in aged rats have lower frequency than those detected in young animals. While CA1 ripples are thought to be driven by CA3, HFEs in CA3 have not been examined in aged animals. The current study obtained simultaneous recordings from CA1 and CA3 in young and aged rats to examine sharp wave/ripples/HFEs in relation to age. While CA1 ripple frequency was reduced with age, there were no age differences in the frequency of CA3 HFEs, although power and length were lower in old animals. While there was a proportion of CA1 ripples that co-occurred with a CA3 HFE, none of the age-related differences in CA1 ripples could be explained by alterations in CA3 HFE characteristics. These findings suggest that age differences in CA1 are not due to altered CA3 activity, but instead reflect distinct mechanisms of ripple generation with age.

[*]Corresponding author at: University of Florida, Neuroscience, McKnight Brain Institute, P.O. Box 100244, 1149 Newell Dr, RM L1-100G, Gainesville, FL 32610, USA. burkes@ufl.edu (S.N. Burke). [**]Corresponding author at: McKnight Brain Institute, 1149 Newell Dr, RM L1-100E, University of Florida, Gainesville, FL 32610, USA. drewmaurer@ufl.edu (A.P. Maurer).
[#]Indicates shared corresponding authorship.

CRediT authorship contribution statement

Nicholas M. DiCola: Conceptualization, Methodology, Software, Formal analysis, Investigation, Data curation, Writing – original draft, Writing – review & editing, Visualization. **Alexa L. Lacy:** Investigation. **Omar J. Bishr:** Investigation. **Kathryn M. Kimsey:** Investigation. **Jenna L. Whitney:** Investigation. **Sarah D. Lovett:** Investigation. **Sara N. Burke:** Conceptualization, Methodology, Formal analysis, Resources, Writing – original draft, Writing – review & editing, Supervision, Project administration, Funding acquisition. **Andrew P. Maurer:** Conceptualization, Methodology, Formal analysis, Resources, Writing – original draft, Writing – review & editing, Supervision, Project administration, Funding acquisition.

Disclosure statement

The authors report no conflicts of interest.

Authors declare that data contained in the manuscript being submitted have not been previously published, have not been submitted elsewhere and will not be submitted elsewhere while under consideration at Neurobiology of Aging.

All authors have reviewed the contents of the manuscript being submitted, approve of its contents and validate the accuracy of the data.

Supplementary materials

Supplementary material associated with this article can be found, in the online version, at doi:10.1016/j.neurobiolaging.2022.04.014.

Keywords

Co-Occurrence; Entorhinal cortex; Local field potential; Rat; Sharp wave; Synapse

1. Introduction

The average life expectancy has outpaced the cognitive health span, with a majority of adults over the age of 65 suffering from disruptions in cognitive abilities (Blazer et al., 2015). One brain region that is well documented as being particularly vulnerable to neurobiological alterations in advanced age is the hippocampus. As such, performance on behavioral tasks that rely on the hippocampus, such as explicit memory (Rosenzweig and Barnes, 2003) and spatial navigation (Lester et al., 2017), are degraded in aged humans (Blazer et al., 2015), monkeys (Rapp et al., 1997), and rodents (Barnes, 1979). Our understanding of the biological mechanisms that account for these deficits, however, is incomplete.

Profound cell loss does not occur in normative aging (West et al., 1994; Rapp and Gallagher, 1996). Thus, the mechanisms of impaired hippocampal function in advanced age must arise from more subtle neurobiological changes that affect synaptic function and neuron signaling to alter the dynamics of neuronal network activity that support behavior (Rosenzweig and Barnes, 2003; Burke and Barnes, 2006). For instance, the evoked field excitatory post-synaptic potential (fEPSP) at the CA3 to CA1 Schaffer collateral synapse is reduced in aged compared to young rats (Landfield et al., 1986; Barnes et al., 1992; Deupree et al., 1993; Tombaugh et al., 2002). Because the pre-synaptic fiber potential of the CA3 Schaffer collaterals to CA1 does not change between young and aged animals (Barnes et al., 1997; Rosenzweig et al., 1997; Barnes et al., 2000; Tombaugh et al., 2002), the number of afferent projections is likely to remain intact. In fact, the decreased fEPSP in advanced age appears to be related to the decline in post-synaptic densities of perforated synapses in CA1 (Nicholson et al., 2004) and impaired temporal summation in CA1 pyramidal neurons (Rosenzweig et al., 1997). Additionally, there are notable age-related changes in the activity properties of CA3 neurons that are likely to impact efferent targets in CA1. These changes include a decrease in interneurons expressing GAD67 (Spiegel et al., 2013), and elevated activity in CA3 excitatory cells (Wilson et al., 2005c; Robitsek et al., 2015; Thomé et al., 2016; Lee et al., 2021). Together, these data suggest that the ability of the CA3 subregion to influence CA1 activity is likely to be altered in advanced age. To our knowledge, however, there have been no investigations regarding whether coordinated activity between CA3 and CA1 is altered as a function of age in awake behaving animals.

One readout of coordinated synaptic activity are oscillations in the local field potential (LFP), which are the superposition of inhibitory and excitatory synaptic events (Buzsaki et al., 1983; Buzsaki et al., 2012). Oscillations in the high frequency range (>120 Hz) (Ylinen et al., 1995), known as ripples, are thought to be the product of mass CA3 depolarization of CA1 pyramidal neurons at the stratum radiatum through the Schaffer collateral synapse. This depolarization event, known as the sharp wave, occurs during slow-wave sleep (Wilson and McNaughton, 1994; Chrobak and Buzsaki, 1996; Skaggs and McNaughton, 1996; Kudrimoti et al., 1999; Nadasdy et al., 1999; Sutherland and McNaughton, 2000; Lee and

Wilson, 2002; Buzsaki et al., 2003; Born et al., 2006; Grosmark et al., 2012; Cox et al., 2020; Laventure and Benchenane, 2020; Ngo et al., 2020; Oyanedel et al., 2020; Skelin et al., 2021) and periods of quiet wakefulness (Buzsaki, 1986; Chrobak and Buzsaki, 1996; Foster and Wilson, 2006; Jackson et al., 2006; O'Neill et al., 2006; Csicsvari et al., 2007; Diba and Buzsaki, 2007; Davidson et al., 2009; Karlsson and Frank, 2009; Sullivan et al., 2011; Buzsáki, 2015; Giri et al., 2019). Therefore, these events could be an in vivo neurophysiological indicator of the integrity of CA3 to CA1 coordination.

Previous work has reported differences in CA1 ripples between young and aged rats (Wiegand et al., 2016; Cowen et al., 2020). In old rats, ripples have a reduced peak frequency compared to young animals and a lowered rate of occurrence after the rats performed a circular running task involving acquisition of an association between a spatial location and eyelid stimulation. These changes in CA1 ripples with age may have implications for cognitive function, as it has been proposed that ripples support memory function (Chrobak and Buzsaki, 1996; Nakashiba et al., 2009; Buzsáki, 2015). They may also reflect synaptic reorganization that occurs during behavior (Foster and Wilson, 2006; Csicsvari et al., 2007; Davidson et al., 2009; Atherton et al., 2015; Buzsáki, 2015; Ambrose et al., 2016; Deng et al., 2016; Cazin et al., 2020), although some findings have challenged that hypothetical role of reactivation during ripples for memory stabilization (Gupta et al., 2010; Kovács et al., 2016). Critically, CA1 ripples are known to require intact inhibitory and excitatory balance (Schlingloff et al., 2014; Stark et al., 2014; Gan et al., 2017). Synchronous sodium spikes in CA3, which occur in association with CA1 ripples, are referred to as High Frequency Events (HFEs). HFEs are also thought to manifest from inhibitory control of pyramidal neurons (Schlingloff et al., 2014). CA3 HFEs are likely to change with age due to disruptions in inhibition within CA3 (Shetty and Turner, 1998; Shi et al., 2004; Stanley and Shetty, 2004) as well as the increased excitation of pyramidal neurons (Wilson et al., 2005c; Lee et al., 2021). Despite these observations of disrupted inhibitory/excitatory balance in CA3, characteristics of HFEs in this region have not been investigated in aged rats. The current experiment was designed to examine the extent that age-related changes in CA1 ripples were related to alterations in CA3 HFEs in vivo during quiet wakefulness or rest.

2. Materials and methods

2.1. Subjects

The current experiments used 10 aged (24–26 month) and 11 young (4–8 month) male, Fischer 344xBrown Norway F1 hybrid rats obtained from the National Institute on Aging (NIA) colony at Charles River. One aged and 2 young rats were excluded for not having simultaneous CA1 and CA3 electrophysiological recordings for a final total of 9 aged and 9 young rats. While the importance of the inclusion of both sexes is recognized, a lack of availability of female rats from the NIA colony during the timeframe that the current data were collected and then the research closure during the COVID-19 pandemic precluded the use of female rats in this study. Upon arrival to the animal colony at the University of Florida, the animals habituated for 1 week before beginning food restriction and behavioral shaping. Rats were restricted to 85% of their *ad lib* weight. In some cases, rats were over

conditioned upon arrival at the colony and 85% of the initial weight was insufficient to motivate appetitive behaviors. This was observed in all the aged rats who arrived at the facility over conditioned with excessive visceral white adipose depots (Hernandez et al., 2018). Thus, throughout the period of restricted feeding, in addition to daily weighing, rats were assessed weekly for a body condition score ranging from 1– 5, with 3 being optimal, 1 being emaciated and 5 being obese. The body condition score is assigned based on the presence of palpable fat deposits over the lumbar vertebrae and pelvic bones (Hickman and Swan, 2010; Ullman-Culleré and Foltz, 1999). Baseline weights were re-set to correspond to the weight of the animal with a body condition score of 3. If rats dropped to a body condition of 2.5 more food was made available. Animals were individually housed and maintained on a reverse 12:12 hour light:dark cycle, with training and neurophysiological recordings occurring during the dark phase. All experiments followed the guidelines of the United States National Institute of Health's *Guide for the Care and Use of Laboratory Animals* and were approved by the University of Florida Institutional Animal Care and Use Committee.

One week after arriving to the animal housing facility rats began habituation to experimenters and the maze environment. They were placed into the room and trained to traverse their respective mazes until they could successfully complete 30 trials in 30 minutes. Cereal marshmallows broken into approximately 0.03–0.1 g pieces were used as a reward. This was followed by object displacement training where the animals learned to move a 6.25 × 6.25 × 5.75 cm square LEGO block in preparation for object discrimination. After successfully reaching criterion on object displacement training, rats were then trained on one or more of several different behavioral tasks: the LEGO discrimination task (Johnson et al., 2017), the Object-Place Paired Association task (Hernandez et al., 2015), or continuous alternation. Not all animals were able to complete all behavioral tasks before the implants were no longer viable or the animal had health complications related to age.

2.2. Surgery and neurophysiology

After reaching criterion, rats were stereotaxically implanted with dual, chronic, high-density silicon probes from Cambridge Neurotech mounted on moveable nano-drives with 5 mm of vertical travel. Three days before surgery, rats were given an anti-biotic regiment that continued until 10 days post-surgery (0.5 mL/d of sulfatrim pediatric suspension: 20 mg Sulfamethoxazole, 4 mg Trimethoprim, no more than 0.5% alcohol by volume). Immediately prior to surgery, all rats were also administered 0.5 mL of Metacam diluted with 0.1 mL of sterile saline and 0.01 mL/100 grams of bodyweight of Atropine diluted with 0.1 mL of sterile saline. Rats were initially put under anesthesia with 5% by volume isoflurane that was then lowered to 1%–2% throughout surgery. Oxygen flow rate was maintained between 1.5–2.0 L/ minute. Group 1 (4 young, 4 aged) was then implanted with dual, F-series silicon probes in the cortex above the hippocampus, with destinations for either CA1 (from bregma and brain surface, most medial shank: Anterior/Posterior −4.0 mm, Medial/Lateral 1.8 mm, Dorsal/Ventral −0.5 mm) or CA3 (from bregma and brain surface, most medial shank: Anterior/Posterior −3.2 mm, Medial/Lateral 2.2 mm, Dorsal/Ventral −1.0 mm). These coordinates were chosen to optimize recording of the CA1 efferents of CA3 pyramidal neurons since CA3 primarily projects posteriorly (Amaral

and Witter, 1995). Group 2 (5 young, 5 aged) received L3 series electrodes above the hippocampus (from bregma and brain surface: Anterior/Posterior −3.2, Medial/Lateral 2.2 mm, Dorsal/Ventral −3.5 mm) and the lateral entorhinal cortex (not analyzed or discussed in this paper). Both probes were purchased from Cambridge Neurotech. The F-series probes had 64 channels across 6 shanks, with each shank spanning approximately 150 μm and each shank spaced 200 μm from its neighbor (Fig. 1A). The L3 series probes had 64 channels linearly spaced 50 μm covering 3.15 mm and was able to record simultaneously from CA1, CA3, and the dentate gyrus (Fig. 1B). While positioning CA1 probes posteriorly to the CA1 probes would have been optimal for all rats due to the posteriorly projecting CA3 axons, this benefit was outweighed by the advantage of the linear probes spanning all hippocampal sub-layers, which allowed the generation of current source density calculations and the precise localization of distinct hippocampal laminae. After a craniotomy was performed at these locations the dura was removed before implanting the probes. A reference electrode was implanted using a steel screw into the cerebellum to remove movement noise. A grounding electrode was placed in the contralateral pre-frontal cortex. After implanting, dura-gel was added to the opening to form a flexible, impermeable layer between the air and brain tissue. In-depth surgical instructions can also be viewed on the website for Cambridge Neurotech (https://www.cambridgeneurotech.com/neural-probes). A copper mesh that surrounded the implant to provide both electrical and physical protection was then placed and affixed with dental cement. The ground wire was soldering to the copper mesh cage. Probes were connected to ZIF clips that were mounted in the dental cement and could be attached to clips that ran to a Tucker Davis Technologies electrophysiology recording hardware sampling data at 24,414.0625 samples/second. After surgery, the rats were given 5 mL of warmed, sterile saline for hydration. Simultaneous video recordings were taken from 2 overhead cameras, one to track LEDs mounted on the ZIF clips to track the animal's location and head direction, and 1 infrared camera for post-run behavioral scoring. Raw data was saved to an external server and a copy was saved in a 4 kHz sampling rate format to an additional external hard drive.

2.3. Behavioral procedures for neurophysiological recordings

Post-surgery, all animals were re-trained to push the square block prior to performing their respective task (LEGO discrimination or OPPA training). All rats performed 2 additional behavioral tasks, an 8-maze alternation and a circular track running task. The 8-maze alternation required the animal to alternate turning direction to receive a reward. Animals completed 50 laps or ran for 60 minutes, whichever came first. The circle task required rats to run in a counterclockwise direction for 50 laps or 60 minutes, whichever came first. 8-Maze alternation data was used to probe for possible age-related cognitive impairments. As all rats did not perform this task, only a portion of the rats were included for behavioral analysis (N_{young}= 6, N_{aged} = 7) Scores were based on the number of errors, or incorrect turning directions, prior to, and including, the rat performing the 8-maze task at an 86% accuracy. All electrophysiology data presented here were analyzed from days in which animals completed the continuous alternation on the 8-maze or circle running, which were selected over others because all rats had performed at least one of these tasks. For all recording days, data was collected during 20-minute rest epochs that flanked the behavioral

testing. All analyses were restricted to the pre- and post-run recording epochs to assess local field potential dynamics during these “offline” periods.

2.4. Detection of high-frequency events

Because there is not a local maximum in the ripple range (~100–300 Hz) of the power spectral densities of the CA3 pyramidal layer, CA3 events in the current study are differentiated from CA1 by using the term CA3 high frequency events (HFE) rather than ripples. Detection and analysis methods, otherwise, did not differ between the regions. The term “events” will refer to both ripples and high frequency events from CA1 and CA3, respectively. Channels were picked that either contained spiking events with burst-firing characteristics, indicating their location in the pyramidal layer, or were chosen based on the direction of the sharp waves. This was easiest to see in the 3.15 mm long, L3 probes (Fig. 2), so the power spectral density of all the channels in the F-series probes were compared to those in the L3. Channel selection was the same across both rest epochs but could change across days. Data was then bandpass filtered between 50 Hz and 300 Hz, rectified, and the mean and standard deviation of the amplitude was calculated. Frequency ranges were selected as the widest frequency range cited in a previous investigation into ripples (Sullivan et al., 2011), as well as the ripple frequency distributions in the current dataset (Fig. 3A–D). Hartigan’s Test for Bi-modality and one-sampled Kolmogorov-Smirnov (KS) tests for distribution normality were computed for each rat’s frequency distribution. Because all rats returned significant KS tests ($p < 0.05$), median values for each rat were used for all of the following analyses. Additionally, because all rats returned non-significant Hartigan’s tests for bimodality ($p > 0.05$), no attempt was made to separate events based on different frequency ranges. To rule out the possibility that a disproportionate false classification of lower frequency events was classified as ripples in aged compared to young rats, we replicated the methods of a previous analysis showing that high frequency hippocampal oscillations were bimodally distributed with a local minima at ~140 Hz, which presumably separated gamma from ripples in CA1 (Sullivan et al., 2011). In short, time series data were filtered between 50 and 250 Hz, and high frequency events with a spectral peak greater than 2 standard deviations above baseline in the 120–200 Hz frequency range were selected for analysis. CA3 events were triggered to those in CA1 and were not detected independently. Frequency was then calculated using multi-taper on 100ms windows. For CA1, the frequency distributions for both young and aged rats had a rather unimodal distribution in the pre-run rest epoch, although it was more skewed in the post-run rest. No distribution passed a Hartigan test for bi-modality ($p > 0.05$), indicating that there was not a disproportionate contamination of gamma in the ripple detections between age groups (Fig. 3E–H).

Event detection thresholds for the rest epochs was based on thresholds set from the run epoch, as previously described (Maurer et al., 2006). Briefly, an event was detected when the rectified signal crossed 3 standard deviations above the mean. The point where the signal fell below 2.5 standard deviations was then designated the start and end of the event. Events with an inter-event interval less than 15 ms were combined. Events shorter than 30 ms or longer than 500 ms were not included in the analysis. To account for noise events such as chewing artifacts, the standard deviation of the ripple (115–250 Hz) and sharp wave (12–40

Hz) power across all channels was calculated. If the ripple and sharp wave power standard deviations did not exceed 3 or 5 from the mean, respectively, that event was considered a false positive and excluded from further analysis. This approach capitalizes on the fact that the localized current sources and sinks within the laminar structure of the hippocampus produce changes in the measured LFP signal across different laminar positions, while noise is typically homogenous across all channels. Event coincidence between CA1 and CA3 was measured from the peak power of the event due to the start being highly variable and based on what thresholds are used.

2.5. Event quantification and analysis

All quantifications were done on the median values of the respective metric for each rat. Sample sizes were based on rat count, not event numbers, to avoid violating the assumption of independent samples and inflating statistical power. Seven metrics were calculated: frequency, power, amplitude, length, and envelope half-width time length. Amplitude and envelope half-width time length are reported in Supplementary Fig. 1 as they were consistent with power and length measures, respectively. Frequency was calculated based on the number of local minimums of the 50–300 Hz band-passed signal divided by the length of the ripple. Power was calculated as the sum of the squared values of the filtered (50–300 Hz) signal divided by the length. Length was described earlier as the time difference between when the envelope of the filtered, rectified signal fell below 2.5 standard deviations of the mean. Amplitude was the maximum absolute value of negative values of the filtered (50–300 Hz) signal. Envelope half-amplitude time width was the time length of the negative envelope at half its maximum amplitude.

Sharp waves were only quantified on the rats in Group 2 that received the L-series electrode arrays (5 young, 5 aged) because they were implanted with the 3.15 mm long probe, which spanned all hippocampal sublayers. The radiatum channel was chosen using the current source density (CSD) during CA1 ripple events that co-occurred with CA3 HFEs. The channel with the largest sink located above the dentate gyrus was considered as the radiatum. This was hand verified using the raw traces. Possible sharp waves were then detected based on the presence of a local maxima in the CSD of the 30 Hz low-passed signal of that channel, and were removed if their power did not surpass 5 standard deviations from the mean CSD power. Sharp wave power was calculated as the sum of the squared, 30 Hz lowpass filtered trace of that channel during selected events. CSD amplitude was the maximum value of the 30 Hz lowpass filtered CSD during selected events.

Principal Component Analysis (PCA) was performed in SPSS on the 3 different metrics of frequency, power, and length. Values for each rat were derived from the median of the combined day 1 and day 2 events. Epochs were kept as separate data points due to the consistent significance with respect to rest epoch, but lack of significant differences across days. There were therefore 2 values for each rat/metric combination. Significant loadings in the PCA matrix were considered those whose absolute value was greater than 0.4. Metrics that loaded significantly onto the same component were then tested for correlations based on their Pearson's Correlation Coefficient and t-statistic using the MATLAB function *corrcoef*. Young and aged rats were analyzed separately as well as combined. A p-critical value was

determined based on a Bonferroni correction for multiple comparisons. Correlations on the raw event data, where every event was its own data point, were also calculated. This was done for verification purposes only and significance testing was not performed on this dataset due to the overpowered nature of the analysis and violation of independence of samples.

Event rates (events/second) were calculated as the number of occurrences in a rest epoch over the length of the rest epoch. For illustrative purposes, event rate and rat speed were also binned into 2-minute blocks (Supplementary Fig. 2).

2.6. Statistical analysis

Mixed Model Analysis of Variances (ANOVA) were used to analyze age differences across multiple rest periods, days, and conditions with 2 between subject factors of age group (young and aged) and familiarity (novel day 1 and familiar day 2). Rest epoch (pre-run rest epoch 1 and post-run rest epoch 3) was the within subjects factor. The CA1 and CA3 regions were analyzed separately. A rejection of the null hypothesis was considered with an alpha level of $p < 0.05$. This design was also used to study event co-occurrence between regions and rat speed. To study event metrics as a function of the co-occurrence between CA1 and CA3, the statistical design was again a mixed model ANOVA but with 2 between subjects factors of age group and rest epoch, and one within subjects factor of event co-occurrence (non-co-occurrence and with co-occurrence). Days and regions were analyzed separately, and significance was set at $p < 0.05$. Event rates were tested for significance using a mixed model design with a between subjects factor of age and region, and a within subjects factor of rest epoch. Days were analyzed separately. Finally, event rates and rat speeds (binned into 2-minute time windows) were examined with a Mixed Model ANOVA with a between subjects factor of age, and within subjects factor of time blocks (df = 9). Rest epochs and days were all analyzed separately.

2.7. Histological probe verification

After all experiments were completed, rats were injected with 0.9 mL of SomnaSol (pentobarbital) and perfused through their left ventricle with 4% para-formaldehyde (PFA). Brains were extracted and suspended in more PFA until cryoprotection with 30% sucrose PBS solution. Once brains lost buoyancy, they were flash frozen with dry ice and embedded in Tissue-Tek Optimal Cutting Temperature compound. Brains were then stored in a −80°C freezer overnight for temperatures to stabilize. The next day the brains were moved to a −20°C freezer overnight. Brains were sectioned onto Fisher Superfrost Plus slides in 50 μm thick slices in a Cryostat kept at −20°C. These slides were stained with Nissl and imaged at 20x magnification for verification of probe placement.

3. Results

3.1. CA1 ripples and CA3 HFE rates were significantly affected by rest epoch but were similar between young and behaviorally impaired aged rats

Event rates were calculated by dividing the number of events in a rest epoch by the rest epoch time. Event rate significantly increased between the pre- and post-run rest epochs in

both CA1 and CA3 for Day 1/Novel ($F_{[1,32]}$ = 37.059, p = 8.42e-7) (Fig. 4A) but not Day 2/Familiar ($F_{[1,32]}$ = 2.21, p = 0.147) (Fig. 4B). Additionally, on the Familiar Day, there were significantly more ripples in CA1 than there were HFEs in CA3 ($F_{[1,32]}$ = 4.47, p = 0.042) that approached, but did not reach, significance on the Novel Day ($F_{[1,32]}$ = 3.78, p = 0.061). The difference in event rates between CA1 and CA3 could be due to differential sensitivity of the detection methods for identifying events or could indicate that CA1 ripples can be generated independently of CA3 HFEs. It is important to note that despite very low rates in some animals, the lowest number of events for any animal was 50 for a 20-minute rest period. Importantly, there was no age effect for either the Novel ($F_{[1,32]}$ = 0.074, p = 0.79) or the Familiar Day ($F_{[1,32]}$ = 0.062, p = 0.81). The age by rest epoch interaction on the Novel Day, however, trended towards being significant (F[1,32] = 3.78, p = 0.055), which is likely due the increase in event rates between epochs being relatively greater in the young compared to aged rats. While the event rate did not vary between age groups, it is notable that movement speed during the rest epochs was significantly greater for young compared to aged rats (F[1,32] = 8.348, p = 0.0069) (Fig. 4C).

To determine if the aged rats showed cognitive differences compared to young animals, we examined the number of errors made during the continuous alternation task prior to animals reaching a criterion performance of 86% correct. Aged rats made significantly more errors than did the young during the 8-maze continuous alternation task (RankSum = 25, p = 0.026) (Fig. 4D). It is therefore conceivable that potential differences in other metrics of CA1 ripples and CA3 HFEs, which will be discussed below, could be related to cognitive status.

3.2. Advanced age had dissociable effects on CA1 ripples and CA3 HFE metrics

Event frequency, power, and length were not normally distributed. Thus, statistics were calculated based on the median of events found within a rest epoch calculated for each rat. Consistent with previous reports of aging on CA1 ripples (Wiegand et al., 2016), CA1 ripple frequency was significantly lower in aged rats compared to young (Fig. 5C; $F_{[1,32]}$ = 6.781, p < 0.05, Mixed Model ANOVA; see Table 1 for a summary of all statistics), though this age effect was not evident for CA3 HFEs. Additionally, age significantly interacted with rest epoch, where aged rats showed a greater increase in CA1 ripple frequency from pre- to post-run rest epochs compared to young rats ($F_{[1,32]}$ = 7.838, p < 0.01). Event power and length were significantly lower in aged compared to young rats for CA3 HFEs, but not for CA1 ripples ($F_{[1,32]}$ >4.157, p < 0.05, for both comparisons) (Fig. 5 F,H). The length of CA3 HFEs also significantly interacted with age and rest epoch ($F_{[1,32]}$ = 5.254, p < 0.05 for both comparisons), such that length decreased between epochs for young rats, but not aged rats. While there was no significant main effect of Novel versus Familiar Days (Day 1 versus Day 2) on any of the measured metrics ($F_{[1,32]}$ <.78, p > 0.38, for all comparisons), Day did significantly interact with rest epoch for both CA1 ripple frequency and power (Fig. 5 C,E) ($F_{[1,32]}$ >5.42, p < 0.05).

To ensure rigor, CA1 ripple and CA3 HFE amplitude and envelop half-amplitude time were also calculated as secondary analyses for power and length, respectively. Consistent with the previous analyses, CA1 ripple amplitude was significantly affected by rest epoch ($F_{[1,32]}$ =

19.22, $p = 0.0001$), and rest epoch interacted with Familiarity ($F_{[1,32]} = 7.98$, $p = 0.008$). Also consistent was the effect of age on CA3 HFE amplitude ($F_{[1,32]} = 6.7$, $p = 0.014$) and rest epoch on CA3 HFE envelope time ($F_{[1,32]} = 6.51$, $p = 0.016$). These metrics can be seen in Supplementary Fig. 1 with summary statistics in Supplementary Table 1.

3.3. CA1 ripple and CA3 HFE metric relationships

To quantify potential relationships between ripple and HFE frequency, power, and length in CA1 and CA3, respectively, event metrics during the pre-run and post-run epochs for both subregions were subjected to principal component analysis (PCA) (Table 2). A PCA with a varimax rotation was performed due to the occurrence of split loadings without the rotation. The rotation converged in 5 iterations. Due to the problematic loadings of CA3 HFE frequency across multiple PCA components (absolute value >0.2), this metric was removed from further correlation testing. According to total variance explained, a model using the top 3 components (eigenvalues >1.0) explained 79.854% of the variance in the event metrics, with the first component accounting for 40.359% of the variance, the second component accounting for 20.265%, and the third 19.230%. However, due to the removal of CA3 frequency from further analysis, only items that loaded significantly onto component 1 (absolute value >0.4) were used for further correlation testing. Item communalities were high (ranging from 0.50–0.97 for all items). CA1 length and CA3 length both loaded positively onto the first component (0.695 and 0.895, respectively), suggesting that event length across hippocampal subregions was related. CA1 power negatively loaded onto the first component (−0.828), suggesting that longer events had reduced power.

Correlation values of event metrics that loaded onto the same components were then determined with a Pearson's correlation coefficient and its accompanying t-statistic for any regions and metrics that loaded greater than 0.4 onto their respective PCA components. Due to the consistent, significant effect of rest epoch across event metrics, but not of Day/Familiarity, rest epoch values were analyzed separately, and days were combined (i.e., one data point would be the median value of all ripple events that occurred for the pre-run rest period on both days of training). Metrics that loaded in the same direction (positive or negative) on the PCA component tended to correlate positively with each other. As CA1 lengths, CA3 lengths, and CA1 power were the only significant but unproblematic loadings, there were 3 combinations of event metrics. In addition to correlations within age groups, the correlation across the combined data was examined as well. Due to the resultant 9 t-test comparisons, a Bonferroni correction was applied for a p-critical value of 0.0055. Fig. 6 shows the scatter plots of rat median values that depict the relationship between the different metrics, with the inset showing the raw data for all ripple and HFE events. Statistics were not calculated for the raw data beyond regression slopes due to the inflated statistical power from the large sample size and a nested design in which independence of events cannot be assumed.

CA1 length and power, despite being the only metrics analyzed within the same region, were the only ones to not contain any significant correlations ($r_{[16]} < -0.327$, $p > 0.186$ for separated age groups, $r_{[34]} = -0.317$, $p = 0.059$ for combined) (Fig. 6A). CA1 power and CA3 length, however, had a significant inverse correlation for both age groups separately as

well as when the data was combined ($r_{[16]} > -0.654$, $p < 0.003$ for separated, $r_{[34]} = -0.668$, $p = 9e\text{-}6$ for combined) (Fig. 6B). This significant, inverse relationship was not reflected in the correlation of the raw data shown in the inset figures, where the relationship was flat. The length correlations of the age and combined groups, however, showed a significant positive correlation for both the median and raw data ($r_{[16]} = 0.815$, $p = 4e\text{-}5$ for aged rats, $r_{[34]} = 0.582$, $p = 0.0002$ for combined). This positive correlation did not reach significance for the young rats alone ($r_{[16]} = 0.27$, $p = 0.28$) (Fig. 6C).

3.4. Behavior and age did not impact the co-occurrence of CA1 and CA3 events

Due to the decreased synaptic efficacy of the Schaffer collaterals (Landfield et al., 1986; Barnes et al., 1992; Deupree et al., 1993; Tombaugh et al., 2002), it is conceivable that aged rats would exhibit a decreased ability of CA3 to drive coordinated activity in CA1. To test for this, event co-occurrence was examined by measuring the cross-region, inter-event interval with respect to CA1 ripples (Fig. 7), and with respect to CA3 HFEs (data not shown). The timing for each event was based on the peak amplitude of the filtered and rectified signal. A CA1-CA3 co-occurring event was considered to take place when the peaks fell within a ±50 ms window, and the summed value between these time points was used for statistical testing. No significant main effect was found for age, Familiarity/Day, or rest epoch, nor was there a significant interaction effect among any of these variables ($F_{[1,32]} < 3.64$, $p > 0.065$, for all comparisons) (Fig. 7E). Similar results were obtained when CA1-CA3 ripple occurrence was measured with respect to CA3 ripples (data not shown).

Although CA1-CA3 event co-occurrence did not vary by age, it is conceivable that ripples and HFEs that coincided would have distinct properties from those that did not, which could reflect differences in synaptic efficacy. To investigate this possibility, event frequency (Fig. 8A/B), power (Fig. 8C/D), and length (Fig. 8E/F) were separated into co-occurring *(Co)* and non-co-occurring *(Non)* for the Novel Day 1 and Familiar Day 2 separately. Only CA3 HFE power on Novel Day 1 (Fig. 8Di), and CA3 HFE length on Familiar Day 2 (Fig. 8Fii) did not significantly vary by co-occurrence. All other event metrics for both CA1 and CA3 had significantly higher values for the events that co-occurred versus when no ripple-HFE co-occurrence was detected ($F_{[1,32]} > 11.02$, $p < 0.0023$, for all comparisons). Table 3 shows the statistics for all comparisons for CA1 ripples and Table 4 shows the statistics for CA3 HFEs. There were no significant interaction effects between age and co-occurrence on frequency, power, or length in either CA1 or CA3 ($F_{[1,32]} < 2.74$, $p > 0.11$, for all comparisons). When events from young and aged rats were directly compared, the significant differences that were detected across all events were still evident when separated by co-occurring versus non-co-occurring. Specifically, CA1 frequency ($F_{[1,32]} = 9.721$, $p = 0.0038$) (Fig. 8Aii), CA3 power ($F_{[1,32]} = 4.686$, $p = 0.038$) (Fig. 8Di), and CA3 length ($F_{[1,32]} = 4.791$, $p = 0.036$) (Fig. 8Fii) were all significantly greater in young compared to aged rats. Together these data suggest that there may be an increased depolarization or afferent drive when CA1 ripples and CA3 HFEs co-occur that lead to enhanced frequency, power and length. This is increased drive, however, is not sufficient to overcome age differences.

3.5. Sharp wave CSD amplitude, but not power, was significantly affected by age

Due to the reported decrease in synaptic efficacy at the CA3 to CA1 Schaffer collateral synapse, sharp waves in the stratum radiatum were examined for a potential age difference. Sharp waves could only be quantified in rats that were implanted with a long electrode array, as the shorter probes did not reach the stratum radiatum. Thus, only rats in Group 2 with the long, linear, silicon probe (Young n = 5; Aged n = 5) were included. The stratum radiatum was determined based on the channel with the largest sink in the current source density (CSD) analysis of the wide-band signal during CA1 ripple events (Fig. 2B). Sharp wave events were then detected based on the power of the lowpass filtered (30 Hz) CSD of the selected channel crossing 5 standard deviations from the mean. Sharp wave power was calculated based on the summed square of the lowpass filtered (30 Hz) LFP signal and the median value for each rat was used for statistical analysis (Fig. 9A). No significant main or interaction effects were found for age group, day, or epoch ($F_{[1,16]} < 3.27$, $p > 0.089$, for all comparisons). Because power calculations can be affected by electrode impedance and small deviations in placement, the current amplitude contributing to the sharp wave was quantified from the CSD. When peak CSD amplitude was examined, the sharp wave associated current sink of the aged rats had significantly lower values than those of young rats ($F_{[1,16]} = 12.98$, $p = 0.0023$) (Fig. 9B). This observation, in the context of similar sharp wave power between age groups, suggests that depolarizing currents in the aged rats are more distributed across dendritic regions than those of young rats. To determine if age-related differences in CSD amplitude could account for the decreased CA1 ripple frequency in age rats, correlation coefficients were calculated for these variables (Fig. 9C). While there was a trend for higher CSD amplitudes to be associated with lower ripple frequencies for both age groups (young: $r_{[9]} = -0.63$, $p = 0.049$; aged: $r_{[9]} = -.0571$, $p = 0.085$), these values did not reach statistical significance with the Bonferroni correction for multiple comparisons (p-critical<0.0167).

4. Discussion

The current study documented high frequency oscillatory event characteristics and dynamics in the CA1 and CA3 hippocampal subregions of young and aged rats. The primary findings were that CA1 ripple frequency and radiatum sharp wave CSD amplitude were significantly lower in aged, cognitively impaired rats compared to young. Additionally, CA3 high frequency event (HFE) power and length were also significantly lower in aged rats relative to young animals. CA1 ripple frequency and power, as well as CA3 HFE length increased between the pre- and post-run rest epochs, with this effect also interacting with age for CA1 frequency and CA3 length. While it is enticing to speculate how differences in ripple/HFE metrics between pre- and post-behavior may be related to cognitive function, these comparisons contain confounds that the current experiment did not control for. For example, prior to behavior the animal was hungry and post-behavior they had consumed food rewards, which likely elevated blood glucose levels. Furthermore, the different rest epochs may have occurred at distinct points in the animals' circadian cycle. As such, we do not make any claims in the current paper regarding the potential cognitive implications of ripple/HFE metrics changing between pre- and post-behavior rest epochs.

When events across subregions were compared, CA3 and CA1 event lengths were significantly, positively correlated with each other for aged rats, but not for young. The only significant interaction between inter-region events for the young rats was between CA3 HFE length and CA1 ripple power. While there was not a significant effect of age on the probability that CA1 and CA3 events would co-occur within ±50 msec of each other, there were notable differences in both CA1 and CA3 event metrics when co-occurrence was detected versus when it was not. Specifically in both age groups, frequency, power, and length were all increased in co-occurring events compared to when co-occurrence was not detected.

Previous work has reported that in CA1 the frequency of the ripple oscillation is significantly decreased in aged compared to young rats in vivo (Wiegand et al., 2016; Cowen et al., 2020), and in slices obtained from young or aged rats (Kouvaros et al., 2015). We replicated this observation and extended it to show that within CA3 there were no significant differences in HFE frequency, however power and length were lower in the aged rats compared to the young. While it is possible that these age-related differences in CA3 HFEs could be related to the lower frequency of CA1 ripples in aged rats, CA3 HFE power and length was not correlated with CA1 ripple frequency. Additional experiments are needed to determine the extent to which the well documented increase in excitability of CA3 pyramidal neurons (Wilson et al., 2005a; Robitsek et al., 2015; Simkin et al., 2015; Thomé et al., 2016; Maurer et al., 2017; Lee et al., 2021) and the disruptions in CA3 inhibition in advanced age (Shetty and Turner, 1998; Shi et al., 2004; Stanley and Shetty, 2004; Spiegel et al., 2013; Thomé et al., 2016) are related to the age differences in CA3 HFE power and length.

Previous experiments that observed increased CA3 pyramidal cell firing rates in aged animals focused on neurophysiological recordings obtained during behavior (Wilson et al., 2005b; Robitsek et al., 2015; Thomé et al., 2016; Liang et al., 2020). There was not an obvious manifestation of hyperactivity in the CA3 HFEs, such as increased power or higher HFE incidence. It is conceivable that CA3 hyperactivity may only be observable during active, “online” behavior. In line with this idea is the observation that acetylcholine levels in the hippocampus of young rats are higher during active behaviors compared to rest (Dudar et al., 1979). Importantly, acetylcholine has been shown to suppress excitatory synaptic transmission in CA3 (Kremin and Hasselmo, 2007). Because functional acetylcholine release is lower in the aged compared to young hippocampus (Shen and Barnes, 1996; Birthelmer et al., 2003; Schweizer et al., 2003), reductions in acetylcholine release in aged animals during waking states when levels should be high, could contribute to CA3 hyperactivity. This hyperactivity may not be detectable during rest, when cholinergic tone is lower overall.

An alternative interpretation is that higher CA3 pyramidal neuron firing rates in aged rats manifest as reduced power and length of the HFEs. Similar to CA1 ripples (Stark et al., 2014), CA3 HFEs are thought to require pyramidal cell-interneuron interactions (Schlingloff et al., 2014). The disrupted interneuron phenotypes in the aged CA3 (Shetty and Turner, 1998; Shi et al., 2004; Stanley and Shetty, 2004; Spiegel et al., 2013; Thomé et al., 2016)

could therefore be related to the lower power and length of aged CA3 HFEs compared to those recorded from young animals.

While the current study replicated previous reports of reduced CA1 ripple frequency with age, no correlation was found between CA1 ripple frequencies and CA3 HFE metrics. This suggests that age-related CA1 ripple differences were not due to CA3 HFE dynamics themselves, but instead perhaps differences in the small network dynamics within CA1 or differences in the synaptic contacts between the Schaffer collaterals and the CA1 stratum radiatum dendritic layer. This finding, along with the known age-related differences in evoked post-synaptic potentials (EPSP) in rats (Landfield et al., 1986; Barnes et al., 1992; Deupree et al., 1993; Tombaugh et al., 2002), motivated an examination of sharp waves in the stratum radiatum. Despite the most common findings of decreased amplitude of the aforementioned EPSPs, sharp wave power did not differ with age, a finding consistent with in vitro investigations of young and aged mice (Kanak et al., 2013). Instead, a significant decrease in the sharp wave CSD peak amplitude of the aged rats was observed, indicating a lower current sink in the aged compared to young rats. The lower current sink in aged compared to young rats could be due to the decrease in post-synaptic densities of perforated synapses in aged rats (Nicholson et al., 2004), or the impaired temporal summation (Rosenzweig et al., 1997). This observed lower CSD amplitude in aged compared to young rats could also mean that the current sink is more distributed across the dendrites. As there have been no stereological electron microscopic interrogation or functional neurophysiological analyses of the stratum oriens or lacunosum moleculare CA1 laminae, the precise mechanisms for the age-related decrease in CSD amplitude remains to be determined.

The relatively low probability of CA1 ripples co-occurring with a CA3 HFE (Fig. 7E) has 2, not mutually exclusive possibilities. First, the average co-occurrence rate of approximately 30% could be due to probe placement and the fact that CA1 ripples have been reported to travel along the septotemporal axis from their site of origin (Patel et al., 2013). In other words, a CA1 ripple could be generated from a CA3 HFE that was not detectable from the recording site. It is also possible that other regions may contribute to CA1 ripple generation. While CA1 ripples are typically considered to be initiated by spontaneous CA3 pyramidal cell firing, other mechanisms of CA1 ripple generation have been reported, such as excitatory input from the subiculum (Imbrosci et al., 2021) or CA2 (Oliva et al., 2016) leading to synchronous depolarization in CA1. To date, the electrophysiological properties of the subiculum and CA2 across the life span are not known and should be examined moving forward.

The lack of an age difference in CA1 ripple-CA3 HFE co-occurrence suggests that CA1-CA3 coordination during rest is largely functionally preserved in advanced age. Moreover, when CA1 and CA3 event metrics were examined in the context of whether or not they co-occurred (±50 ms) with an event in the other region (Fig. 8), there were also no significant differences with age. Almost all examined event metrics, however, had higher values when there was CA1 ripple-CA3 HFE co-occurrence compared to when co-occurrence was not detected. A possible explanation for this observation is that CA1 ripples that did not co-occur with a detected CA3 HFE were due to those generated by the subiculum or CA2.

Alternatively, it is also possible that CA1 ripples that did not co-occur with a CA3 HFE were ripples that traveled along the septotemporal axis of the hippocampus (Patel et al., 2013), rather than being locally generated. Ripples or HFEs that travel are likely to be lower in frequency, amplitude and length.

4.1. Limitations

The current study has several limitations that should be noted. First, the experimental design did not directly allow high frequency oscillatory events to be related to cognitive performance, as rats were not participating in a hippocampus-dependent behavior during neurophysiological recordings. Second, while the 64-channel longitudinal recording shanks enabled current source density analysis for channel localization, they did not permit single unit spiking activity from individual neurons to be recorded. As a result, analyses could not be complimented by neuron spiking data. Thus, it is not possible to fully interrogate the potential relationship between CA3 hyperactivity in aged animals and rest-related ripple and HFE activity. Third, as is the case when attempting to identify any phenomenon when noise is present, thresholds for detection must be chosen by the experimenters that can alter the results of the analysis. While this is a regrettable reality of signal detection, it is the author's hope that by basing their thresholds on both results observed *a priori* of frequency threshold values (Fig. 3) and prior literature, and disclosing all chosen values for replication, concerns of false positive results due to arbitrary threshold selection can be dissuaded. Finally, due to the long and arduous nature of in vivo neurophysiological recordings from young and aged animals, the sample size of the current experiments it relatively small. We plan to make this data available to other investigators that may want to combine them with additional data for the purpose of replication, increasing power by collating data across labs, or secondary analyses.

Supplementary Material

Refer to Web version on PubMed Central for supplementary material.

Acknowledgements

This work was supported by the McKnight Brain Research Foundation (SNB and APM), NIH/NIA grants AG055544 (APM) and 1RF1AG049722 (SNB), and the McKnight Brain Institute and the NIH T32AG061892 (NMD).

Special thanks to Michael Burke for apparatus construction.

References

Amaral D, Witter M, 1995. Hippocampal formation. In: The Rat Nervous System Academic Press, San Diego, pp. 443–486.

Ambrose RE, Pfeiffer BE, Foster DJ, 2016. Reverse replay of hippocampal place cells is uniquely modulated by changing reward. Neuron 91, 1124–1136. [PubMed: 27568518]

Atherton LA, Dupret D, Mellor JR, 2015. Memory trace replay: the shaping of memory consolidation by neuromodulation. Trends Neurosci 38, 560–570. [PubMed: 26275935]

Barnes CA, 1979. Memory deficits associated with senescence: a neurophysiological and behavioral study in the rat. J Comp Physiol Psychol 93, 74–104. [PubMed: 221551]

Barnes CA, Rao G, Shen J, 1997. Age-related decrease in the N-methyl-D-as-partateR-mediated excitatory postsynaptic potential in hippocampal region CA1. Neurobiol Aging 18, 445–452. [PubMed: 9330977]

Barnes CA, Rao G, Orr G, 2000. Age-related decrease in the Schaffer collateral-e-voked EPSP in awake, freely behaving rats. Neural Plast 7, 167–178. [PubMed: 11147459]

Barnes CA, Rao G, Foster TC, McNaughton BL, 1992. Region-specific age effects on AMPA sensitivity: electrophysiological evidence for loss of synaptic contacts in hippocampal field CA1. Hippocampus 2, 457–468. [PubMed: 1284976]

Birthelmer A, Stemmelin J, Jackisch R, Cassel JC, 2003. Presynaptic modulation of acetylcholine, noradrenaline, and serotonin release in the hippocampus of aged rats with various levels of memory impairments. Brain Res Bull 60, 283–296. [PubMed: 12754090]

Blazer DG, Yaffe K, Liverman CT, 2015. Cognitive Aging: Progress in Understanding and Opportunities for Action National Academies Press, Washington, DC.

Born J, Rasch B, Gais S, 2006. Sleep to remember. Neuroscientist 12, 410– 424. [PubMed: 16957003]

Burke SN, Barnes CA, 2006. Neural plasticity in the ageing brain. Nat Rev Neurosci 7, 30–40. [PubMed: 16371948]

Buzsaki G, 1986. Hippocampal sharp waves: their origin and significance. Brain Res 398, 242–252. [PubMed: 3026567]

Buzsaki G, Leung LW, Vanderwolf CH, 1983. Cellular bases of hippocampal EEG in the behaving rat. Brain Res 287, 139–171. [PubMed: 6357356]

Buzsaki G, Anastassiou CA, Koch C, 2012. The origin of extracellular fields and currents–EEG, ECoG, LFP and spikes. Nat Rev Neurosci 13, 407–420. [PubMed: 22595786]

Buzsaki G, Buhl DL, Harris KD, Csicsvari J, Czeh B, Morozov A, 2003. Hippocampal network patterns of activity in the mouse. Neuroscience 116, 201–211. [PubMed: 12535953]

Buzsáki G, 2015. Hippocampal sharp wave-ripple: a cognitive biomarker for episodic memory and planning. Hippocampus 25, 1073–1188. [PubMed: 26135716]

Cazin N, Scleidorovich P, Weitzenfeld A, Dominey PF, 2020. Real-time sensory-motor integration of hippocampal place cell replay and prefrontal sequence learning in simulated and physical rat robots for novel path optimization. Biol Cybern 114, 249–268. [PubMed: 32095878]

Chrobak JJ, Buzsaki G, 1996. High-frequency oscillations in the output networks of the hippocampal-entorhinal axis of the freely behaving rat. J Neurosci 16, 3056–3066. [PubMed: 8622135]

Cowen SL, Gray DT, Wiegand JL, Schimanski LA, Barnes CA, 2020. Age-as-sociated changes in waking hippocampal sharp-wave ripples. Hippocampus 30, 28–38. [PubMed: 29981255]

Cox R, Rüber T, Staresina BP, Fell J, 2020. Sharp wave-ripples in human amygdala and their coordination with hippocampus during NREM sleep. Cereb Cortex Commun 1 (1), tgaa051 tgaa051.

Csicsvari J, O'Neill J, Allen K, Senior T, 2007. Place-selective firing contributes to the reverse-order reactivation of CA1 pyramidal cells during sharp waves in open-field exploration. Eur J Neurosci 26, 704–716. [PubMed: 17651429]

Davidson TJ, Kloosterman F, Wilson MA, 2009. Hippocampal replay of extended experience. Neuron 63, 497–507. [PubMed: 19709631]

Deng X, Liu DF, Karlsson MP, Frank LM, Eden UT, 2016. Rapid classification of hippocampal replay content for real-time applications. J Neurophysiol 116, 2221–2235. [PubMed: 27535369]

Deupree DL, Bradley J, Turner DA, 1993. Age-related alterations in potentiation in the CA1 region in F344 rats. Neurobiol Aging 14, 249–258. [PubMed: 8321393]

Diba K, Buzsaki G, 2007. Forward and reverse hippocampal place-cell sequences during ripples. Nat Neurosci 10, 1241–1242. [PubMed: 17828259]

Dudar J, Whishaw I, Szerb J, 1979. Release of acetylcholine from the hippocampus of freely moving rats during sensory stimulation and running. Neuropharmacology 18, 673–678. [PubMed: 492487]

Foster DJ, Wilson MA, 2006. Reverse replay of behavioural sequences in hippocampal place cells during the awake state. Nature 440, 680–683. [PubMed: 16474382]

Gan J, Weng SM, Pernía-Andrade AJ, Csicsvari J, Jonas P, 2017. Phase-locked inhibition, but not excitation, underlies hippocampal ripple oscillations in awake mice in vivo. Neuron 93, 308–314. [PubMed: 28041883]

Giri B, Miyawaki H, Mizuseki K, Cheng S, Diba K, 2019. Hippocampal reactivation extends for several hours following novel experience. J Neurosci 39, 866–875. [PubMed: 30530857]

Grosmark AD, Mizuseki K, Pastalkova E, Diba K, Buzsáki G, 2012. REM sleep reorganizes hippocampal excitability. Neuron 75, 1001–1007. [PubMed: 22998869]

Gupta AS, van der Meer MA, Touretzky DS, Redish AD, 2010. Hippocampal replay is not a simple function of experience. Neuron 65, 695–705. [PubMed: 20223204]

Hernandez AR, Hernandez CM, Campos KT, Truckenbrod LM, Sakarya Y, McQuail JA, Carter CS, Bizon JL, Maurer AP, Burke SN, 2018. The Antiepileptic Ketogenic Diet Alters Hippocampal Transporter Levels and Reduces Adiposity in Aged Rats. J Gerontol A Biol Sci Med Sci 73, 450–458. [PubMed: 29040389]

Hernandez AR, Maurer AP, Reasor JE, Turner SM, Barthle SE, Johnson SA, Burke SN, 2015. Age-related impairments in object-place associations are not due to hippocampal dysfunction. Behav Neurosci 129, 599–610. [PubMed: 26413723]

Hickman DL, Swan M, 2010. Use of a body condition score technique to assess health status in a rat model of polycystic kidney disease. J Am Assoc Lab Anim 49, 155–159.

Imbrosci B, Nitzan N, McKenzie S, Donoso JR, Swaminathan A, Böhm C, Maier N, Schmitz D, 2021. Subiculum as a generator of sharp wave-ripples in the rodent hippocampus. Cell Rep 35, 109021. [PubMed: 33882307]

Jackson JC, Johnson A, Redish AD, 2006. Hippocampal sharp waves and reactivation during awake states depend on repeated sequential experience. J Neurosci 26, 12415–12426. [PubMed: 17135403]

Johnson SA, Turner SM, Santacroce LA, Carty KN, Shafiq L, Bizon JL, Maurer AP, Burke SN, 2017. Rodent age-related impairments in discriminating perceptually similar objects parallel those observed in humans. Hippocampus 27, 759–776. [PubMed: 28342259]

Kanak DJ, Rose GM, Zaveri HP, Patrylo PR, 2013. Altered network timing in the CA3-CA1 circuit of hippocampal slices from aged mice. PLoS One 8, e61364. [PubMed: 23593474]

Karlsson MP, Frank LM, 2009. Awake replay of remote experiences in the hippocampus. Nat Neurosci 12, 913–918. [PubMed: 19525943]

Kouvaros S, Kotzadimitriou D, Papatheodoropoulos C, 2015. Hippocampal sharp waves and ripples: effects of aging and modulation by NMDA receptors and L– type Ca2+ channels. Neuroscience 298, 26–41. [PubMed: 25869622]

Kovács KA, O'Neill J, Schoenenberger P, Penttonen M, Ranguel Guerrero DK, Csicsvari J, 2016. Optogenetically blocking sharp wave ripple events in sleep does not interfere with the formation of stable spatial representation in the CA1 area of the hippocampus. PLoS One 11, e0164675. [PubMed: 27760158]

Kremin T, Hasselmo ME, 2007. Cholinergic suppression of glutamatergic synaptic transmission in hippocampal region CA3 exhibits laminar selectivity: implication for hippocampal network dynamics. Neuroscience 149, 760–767. [PubMed: 17964734]

Kudrimoti HS, Barnes CA, McNaughton BL, 1999. Reactivation of hippocampal cell assemblies: effects of behavioral state, experience, and EEG dynamics. J Neurosci 19, 4090–4101. [PubMed: 10234037]

Landfield PW, Pitler TA, Applegate MD, 1986. The effects of high Mg2+-to-Ca2+ ratios on frequency potentiation in hippocampal slices of young and aged rats. J Neurophysiol 56, 797–811. [PubMed: 3783221]

Laventure S, Benchenane K, 2020. Validating the theoretical bases of sleep reactivation during sharp-wave ripples and their association with emotional valence. Hippocampus 30, 19–27. [PubMed: 31334590]

Lee AK, Wilson MA, 2002. Memory of sequential experience in the hippocampus during slow wave sleep. Neuron 36, 1183–1194. [PubMed: 12495631]

Lee H, Wang Z, Zeger SL, Gallagher M, Knierim JJ, 2021. Heterogeneity of age-related neural hyperactivity along the CA3 transverse axis. J Neurosci 41, 663–673. [PubMed: 33257325]

Lester AW, Moffat SD, Wiener JM, Barnes CA, Wolbers T, 2017. The aging navigational system. Neuron 95, 1019–1035. [PubMed: 28858613]

Liang X, Hsu LM, Lu H, Ash JA, Rapp PR, Yang Y, 2020. Functional connectivity of hippocampal CA3 predicts neurocognitive aging via CA1-frontal circuit. Cereb Cortex 30, 4297–4305. [PubMed: 32239141]

Maurer AP, Cowen SL, Burke SN, Barnes CA, McNaughton BL, 2006. Phase precession in hippocampal interneurons showing strong functional coupling to individual pyramidal cells. J Neurosci 26, 13485–13492. [PubMed: 17192431]

Maurer AP, Johnson SA, Hernandez AR, Reasor J, Cossio DM, Fertal KE, Mizell JM, Lubke KN, Clark BJ, Burke SN, 2017. Age-related changes in lateral entorhinal and CA3 neuron allocation predict poor performance on object discrimination. Front Syst Neurosci 11, 49. [PubMed: 28713251]

Nadasdy Z, Hirase H, Czurko A, Csicsvari J, Buzsaki G, 1999. Replay and time compression of recurring spike sequences in the hippocampus. J Neurosci 19, 9497–9507. [PubMed: 10531452]

Nakashiba T, Buhl DL, McHugh TJ, Tonegawa S, 2009. Hippocampal CA3 output is crucial for ripple-associated reactivation and consolidation of memory. Neuron 62, 781–787. [PubMed: 19555647]

Ngo HV, Fell J, Staresina B, 2020. Sleep spindles mediate hippocampal-neocortical coupling during long-duration ripples. Elife 9.

Nicholson DA, Yoshida R, Berry RW, Gallagher M, Geinisman Y, 2004. Reduction in size of perforated postsynaptic densities in hippocampal axo-spinous synapses and age-related spatial learning impairments. J Neurosci 24, 7648–7653. [PubMed: 15342731]

O'Neill J, Senior T, Csicsvari J, 2006. Place-selective firing of CA1 pyramidal cells during sharp wave/ripple network patterns in exploratory behavior. Neuron 49, 143–155. [PubMed: 16387646]

Oliva A, Fernández-Ruiz A, Buzsáki G, Berényi A, 2016. Role of hippocampal CA2 region in triggering sharp-wave ripples. Neuron 91, 1342–1355. [PubMed: 27593179]

Oyanedel CN, Durán E, Niethard N, Inostroza M, Born J, 2020. Temporal associations between sleep slow oscillations, spindles and ripples. Eur J Neurosci 52, 4762–4778. [PubMed: 32654249]

Patel J, Schomburg EW, Berenyi A, Fujisawa S, Buzsaki G, 2013. Local generation and propagation of ripples along the septotemporal axis of the hippocampus. J Neurosci 33, 17029–17041. [PubMed: 24155307]

Rapp PR, Gallagher M, 1996. Preserved neuron number in the hippocampus of aged rats with spatial learning deficits. Proc Natl Acad Sci U S A 93, 9926–9930. [PubMed: 8790433]

Rapp PR, Kansky MT, Roberts JA, 1997. Impaired spatial information processing in aged monkeys with preserved recognition memory. Neuroreport 8, 1923–1928. [PubMed: 9223078]

Robitsek J, Ratner MH, Stewart T, Eichenbaum H, Farb DH, 2015. Combined administration of levetiracetam and valproic acid attenuates age-related hyperactivity of CA3 place cells, reduces place field area, and increases spatial information content in aged rat hippocampus. Hippocampus 25, 1541–1555. [PubMed: 25941121]

Rosenzweig ES, Barnes CA, 2003. Impact of aging on hippocampal function: plasticity, network dynamics, and cognition. Prog Neurobiol 69, 143–179. [PubMed: 12758108]

Rosenzweig ES, Rao G, McNaughton BL, Barnes CA, 1997. Role of temporal summation in age-related long-term potentiation-induction deficits. Hippocampus 7, 549–558. [PubMed: 9347351]

Schlingloff D, Káli S, Freund TF, Hájos N, Gulyás AI, 2014. Mechanisms of sharp wave initiation and ripple generation. J Neurosci 34, 11385–11398. [PubMed: 25143618]

Schweizer T, Birthelmer A, Lazaris A, Cassel JC, Jackisch R, 2003. 3,4-DAP-e-voked transmitter release in hippocampal slices of aged rats with impaired memory. Brain Res Bull 62, 129–136. [PubMed: 14638386]

Shen J, Barnes CA, 1996. Age-related decrease in cholinergic synaptic transmission in three hippocampal subfields. Neurobiol Aging 17, 439–451. [PubMed: 8725906]

Shetty AK, Turner DA, 1998. Hippocampal interneurons expressing glutamic acid decarboxylase and calcium-binding proteins decrease with aging in Fischer 344 rats. J Comp Neurol 394, 252–269. [PubMed: 9552130]

Shi L, Argenta AE, Winseck AK, Brunso-Bechtold JK, 2004. Stereological quantification of GAD-67-immunoreactive neurons and boutons in the hippocampus of middle-aged and old Fischer 344 x Brown Norway rats. J Comp Neurol 478, 282–291. [PubMed: 15368530]

Simkin D, Hattori S, Ybarra N, Musial TF, Buss EW, Richter H, Oh MM, Nicholson DA, Disterhoft JF, 2015. Aging-related hyperexcitability in CA3 pyramidal neurons is mediated by enhanced A-type K+ channel function and expression. J Neurosci 35, 13206–13218. [PubMed: 26400949]

Skaggs WE, McNaughton BL, 1996. Replay of neuronal firing sequences in rat hippocampus during sleep following spatial experience. Science 271, 1870–1873. [PubMed: 8596957]

Skelin I, Zhang H, Zheng J, Ma S, Mander BA, Kim McManus O, Vadera S, Knight RT, McNaughton BL, Lin JJ, 2021. Coupling between slow waves and sharp-wave ripples engages distributed neural activity during sleep in humans. Proc Natl Acad Sci U S A 118 (21), e2012075118. [PubMed: 34001599]

Spiegel AM, Koh MT, Vogt NM, Rapp PR, Gallagher M, 2013. Hilar interneuron vulnerability distinguishes aged rats with memory impairment. J Comp Neurol 521, 3508–3523. [PubMed: 23749483]

Stanley DP, Shetty AK, 2004. Aging in the rat hippocampus is associated with widespread reductions in the number of glutamate decarboxylase-67 positive interneurons but not interneuron degeneration. J Neurochem 89, 204–216. [PubMed: 15030405]

Stark E, Roux L, Eichler R, Senzai Y, Royer S, Buzsáki G, 2014. Pyramidal cell-interneuron interactions underlie hippocampal ripple oscillations. Neuron 83, 467–480. [PubMed: 25033186]

Sullivan D, Csicsvari J, Mizuseki K, Montgomery S, Diba K, Buzsaki G, 2011. Relationships between hippocampal sharp waves, ripples, and fast gamma oscillation: influence of dentate and entorhinal cortical activity. J Neurosci 31, 8605–8616. [PubMed: 21653864]

Sutherland GR, McNaughton B, 2000. Memory trace reactivation in hippocampal and neocortical neuronal ensembles. Curr Opin Neurobiol 10, 180–186. [PubMed: 10753801]

Thomé A, Gray DT, Erickson CA, Lipa P, Barnes CA, 2016. Memory impairment in aged primates is associated with region-specific network dysfunction. Mol Psychiatry 21, 1257–1262. [PubMed: 26503764]

Tombaugh GC, Rowe WB, Chow AR, Michael TH, Rose GM, 2002. Theta-frequency synaptic potentiation in CA1 in vitro distinguishes cognitively impaired from unimpaired aged Fischer 344 rats. J Neurosci 22, 9932–9940. [PubMed: 12427850]

Ullman-Culleré MH, Foltz CJ, 1999. Body condition scoring: a rapid and accurate method for assessing health status in mice. Lab Anim Sci 49, 319–323. [PubMed: 10403450]

West MJ, Coleman PD, Flood DG, Troncoso JC, 1994. Differences in the pattern of hippocampal neuronal loss in normal ageing and Alzheimer's disease. Lancet 344, 769–772. [PubMed: 7916070]

Wiegand JP, Gray DT, Schimanski LA, Lipa P, Barnes CA, Cowen SL, 2016. Age is associated with reduced sharp-wave ripple frequency and altered patterns of neuronal variability. J Neurosci 36, 5650–5660. [PubMed: 27194342]

Wilson I, Ikonen S, Gallagher M, Eichenbaum H, Tanila H, 2005a. Age-associated alterarions in place cells are subregion specific. J Neurosci 25, 6877–6886. [PubMed: 16033897]

Wilson IA, Ikonen S, Gallagher M, Eichenbaum H, Tanila H, 2005b. Age-associated alterarions in place cells are subregion specific. J Neurosci 25, 6877–6886. [PubMed: 16033897]

Wilson IA, Ikonen S, Gallagher M, Eichenbaum H, Tanila H, 2005c. Age-associated alterations of hippocampal place cells are subregion specific. J Neurosci 25, 6877–6886. [PubMed: 16033897]

Wilson MA, McNaughton BL, 1994. Reactivation of hippocampal ensemble memories during sleep. Science 265, 676–679. [PubMed: 8036517]

Ylinen A, Bragin A, Nadasdy Z, Jando G, Szabo I, Sik A, Buzsaki G, 1995. Sharp wave-associated high-frequency oscillation (200 Hz) in the intact hippocampus: network and intracellular mechanisms. J Neurosci 15, 30–46. [PubMed: 7823136]

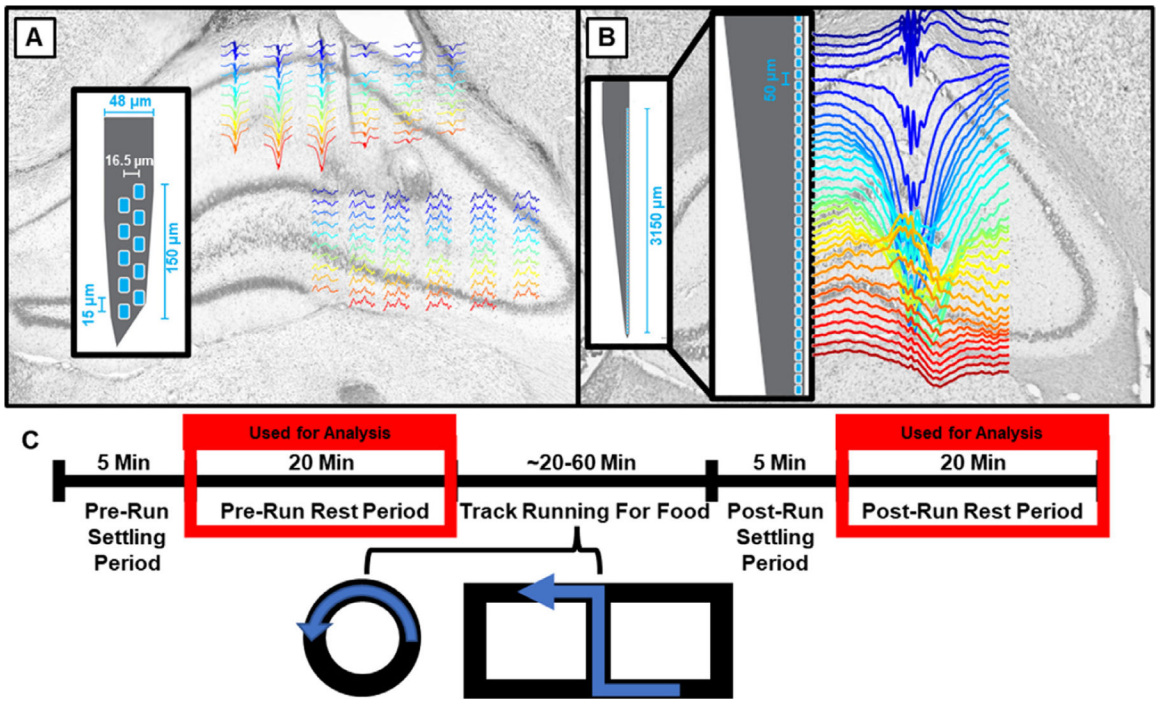

Fig. 1.

Representative sharp wave/ripples overlayed on hippocampal histology along-side probe array configuration and experimental paradigm. The change in the direction of the sharp waves, and the power of the ripple, across the hippocampal layers should be noted for both probe types. Rats with two different electrode arrays were included in the current study: one group with dual silicon probes in the CA1 and CA3 sublayers (A), and the other group had a single linear probe spanning 3 mm (B). Color corresponds to the depth of the probes in the brain for a given array, with warmer colors being more ventral. (C) While rats were run on one of two tracks, only the rest periods were used for analysis. Each rest epoch came after a 5-min settling period that allowed the rat time to calm down after being put in the testing room or running on the track. “(For interpretation of the references to color in this figure legend, the reader is referred to the Web version of this article.)”

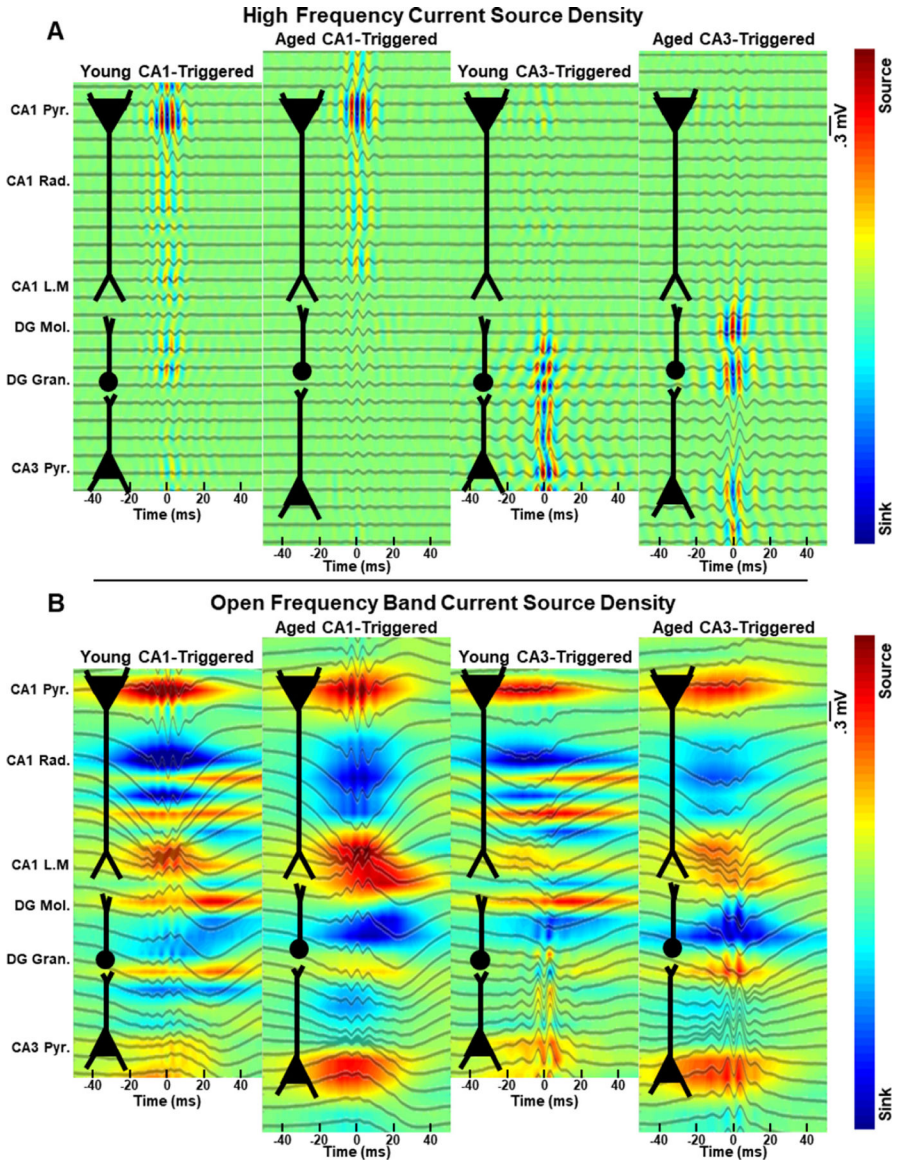

Fig. 2.

Representative traces and current source densities (CSD). CSDs of high frequency event filtered **(A)** and unfiltered **(B)** LFP for young and aged rats triggered on either ripples in CA1 or high frequency events (HFE) in CA3. Traces are shifted to align the CA1 and CA3 layers between rats to show the anatomy aligned with the neurophysiology. Neuronal sub-layers are indicated to the left of the figures. Note the presence of sources and sinks in the pyramidal layer during periods of ripples triggered in the other region (e.g., CA1 ripples during CA3 triggered events). Also evident is the presence of sources and sinks in the molecular layer during pyramidal layer triggered events. Pyramidal layers were identified by spiking activity, radiatum by the first large sink below the CA1 pyramidal layer, lacunosum moleculare and dentate gyrus molecular layer by CSDs triggered to theta (6–12 Hz) or gamma (40–100 Hz) (respectively) during the run epoch (not shown). “(For interpretation of

the references to color in this figure legend, the reader is referred to the Web version of this article.)”

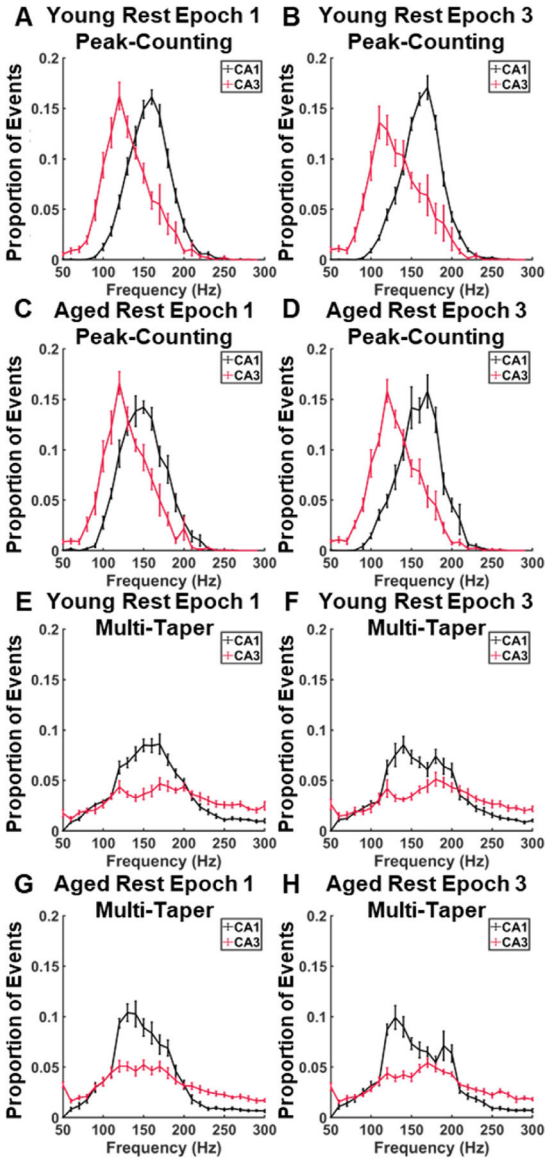

Fig. 3.

Frequency distributions of candidate events calculated using peak counting and multi-taper. Frequency distributions were calculated separately for each rat and averaged (young n = 9; aged n = 9). Error bars are standard error of the means for 10 Hz bins. Hartigan's dip test for bimodality was calculated using 500 bootstraps for each rat. All rats failed to reject the null hypothesis of a unimodal distribution ($p > 0.05$). Additionally, frequency distributions were tested for normality using a one-sampled Kolmogorov-Smirnov test. The null hypothesis of normality was rejected for all rats ($p < 0.05$). Due to the lack of a normal distribution all metrics were calculated using the median for each rat rather than the mean. While other labs have reported a high gamma frequency (90–140 Hz) in the CA1 pyramidal layer (Sullivan et al., 2011) this was not found using the peak-counting method used to calculate ripple frequency **(A–D)**. To rule out the possibility of a false negative, ripples were detected, curated, and frequencies calculated using the methods described in Sullivan et al., 2011 **(E–**

H). In short, CA1 ripples were detected and curated based on the presence of a spectral peak between 120–200 Hz that was significantly larger than the background power spectrum, and frequencies were calculated using a multi-taper method on 100 ms windows. CA3 events were not found independently from CA1. Both methods revealed peak frequency differences in CA1 that were higher relative to CA3, thought the multi-taper method returned a much higher variance of peak frequencies for both regions. “(For interpretation of the references to color in this figure legend, the reader is referred to the Web version of this article.)”

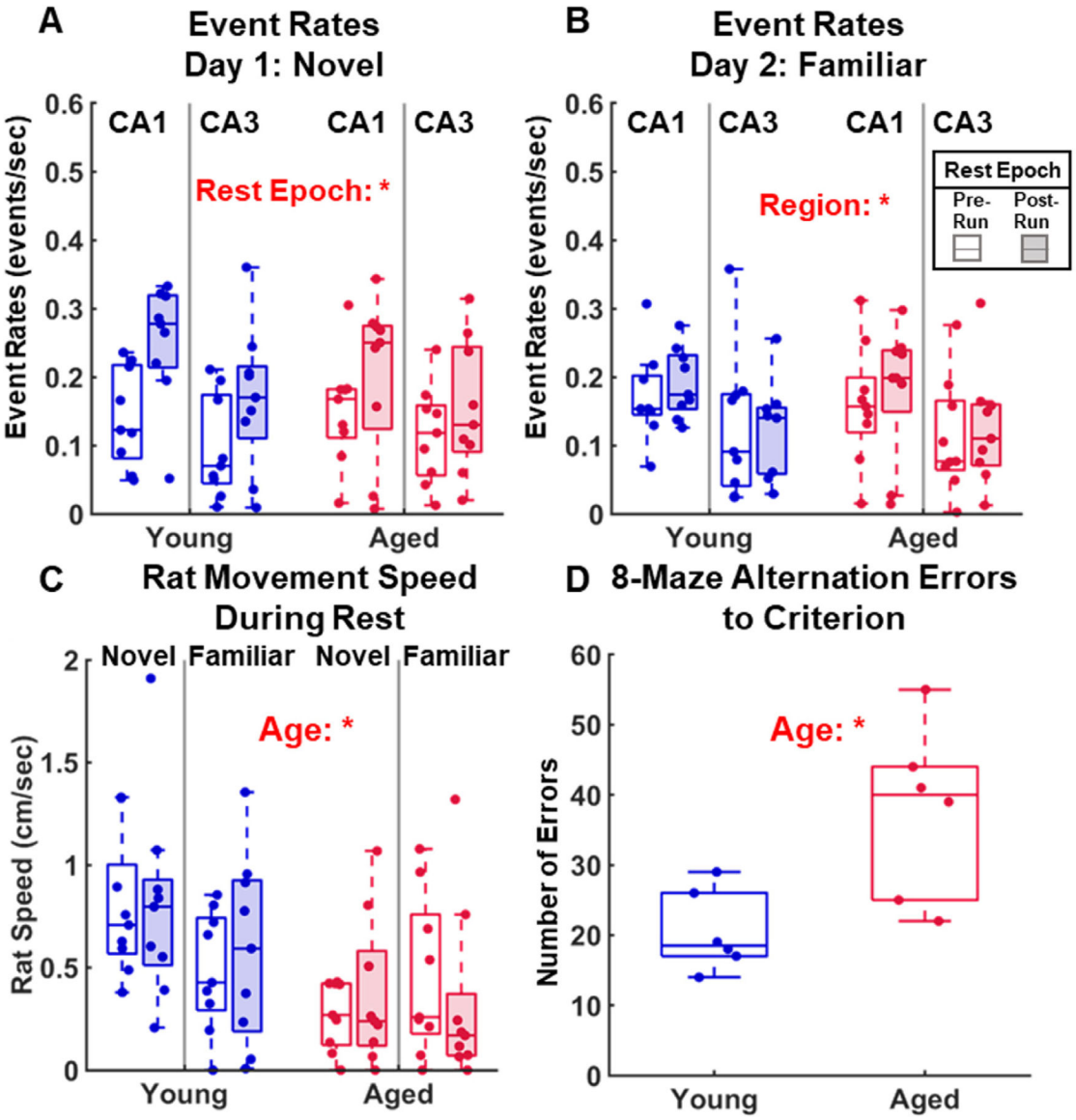

Fig. 4.

CA1 Ripple and CA3 High Frequency Event (HFE) Rate, rat movement speed and cognitive status. (A,B) Median event rates for Day 1 and Day 2 by rest epoch for CA1 and CA3. There was a significant effect of rest epoch only for Day 1 ($F_{[1,32]}$ = 37.059, p = 8.42e-7) but not day 2 ($F_{[1,32]}$ = 2.21, p = 0.147). There was a significant effect of region on Day 2 ($F_{[1,32]}$ = 4.47, p = 0.042) that also trended towards significance on Day 1 ($F_{[1,32]}$ = 3.78, p = 0.061). There was no age effect for either Day 1 ($F_{[1,32]}$ = 0.074, p = 0.79) or Day 2 ($F_{[1,32]}$ = 0.062, p = 0.81), however the age by rest epoch interaction on Day 1 approached significance ($F_{[1,32]}$ = 3.78, p = 0.055). **(C)** Rat speed calculated for both days and rest epochs. Aged rats had a lower average speed during rest than young rats ($F_{[1,32]}$ = 8.348, p = 0.0069), which suggests that young rats moved more during rest. **(D)** For rats that ran the 8-maze alternation task (N_{young} = 6, N_{aged} = 6), the number of errors until they reached a criterion of 86% correct was significant greater in the aged rats relative to the young animals (RankSum = 25,

$p = 0.026$). “(For interpretation of the references to color in this figure legend, the reader is referred to the Web version of this article.)”

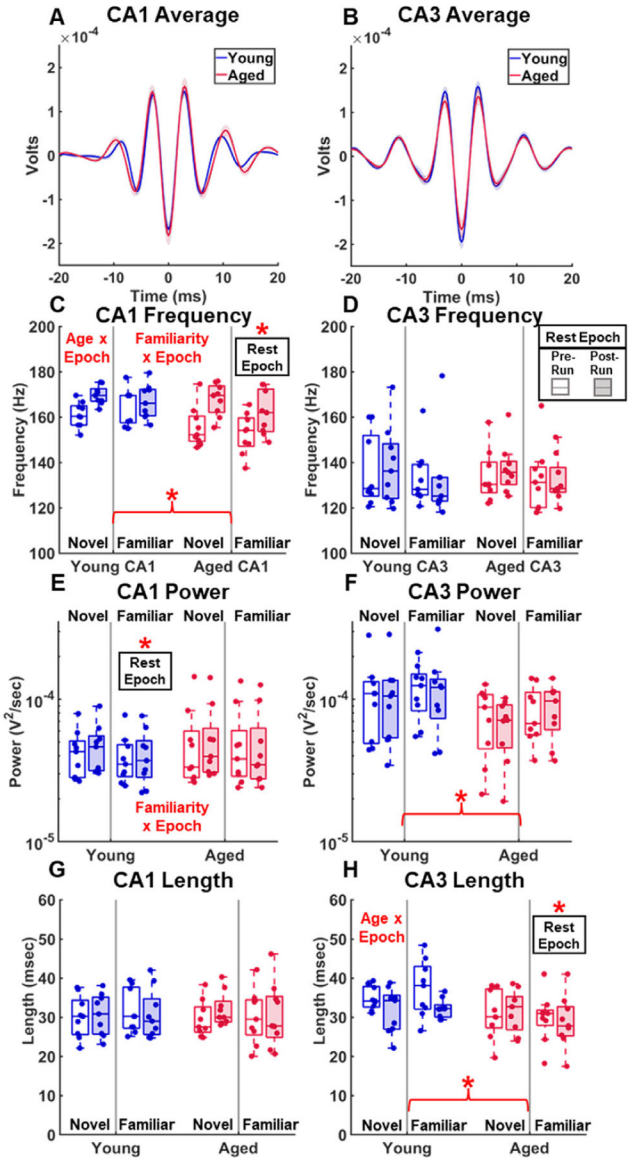

Fig. 5.

Quantification of CA1 Ripples and CA3 High-Frequency Events (HFE). (A–B) Averaged, overlayed, filtered events. The peaks of the young and aged CA1 average ripples diverged while those in the CA3 HFEs did not. **(C, D)** Event frequency separated by region, age, Day (novel versus familiar), and rest epoch. CA1 ripples were significantly different between age groups ($F_{[1,32]} = 6.781$, $p < 0.05$), and rest epoch ($F_{[1,32\ ]} = 70.053$, $p < 0.0001$). The rest epoch and age interaction was also significant ($F_{[1,32]} = 7.838$, $p < 0.01$), as was the rest epoch and Familiarity (Novel Day 1 vs. Day 2; $F_{[1,32\ ]} = 5.748$, $p < 0.05$). CA3 HFE frequency had no significant differences between age groups, epoch or Familiarity. Unshaded boxes indicate pre-run rest, and shaded boxes post-run rest. Significance ($p < 0.05$) was indicated by an asterisk regardless of degree of significance. **(E–F)** CA1 ripple power had significant variation between different rest epochs ($F_{[1,32]} = 7.167$, $p < 0.05$), with a significant interaction effect of rest epochs and familiarity ($F_{[1,32]} = 5.417$, $p < 0.05$). CA3

HFEs exhibited a significant difference between young and aged rats ($F_{[1,32]} = 4.157$, $p < 0.05$) . **(G–H)** CA1 ripple length did not vary for any tested metrics. CA3 HFEs, however, showed significant differences between age groups ($F_{[1,32]} = 5.033$, $p < 0.05$) and rest epochs ($F_{[1,32]} = 8.020$, $p < 0.01$), as well as an interaction effect between the two ($F_{[1,32]} = 5.254$, $p < 0.05$). “(For interpretation of the references to color in this figure legend, the reader is referred to the Web version of this article.)”

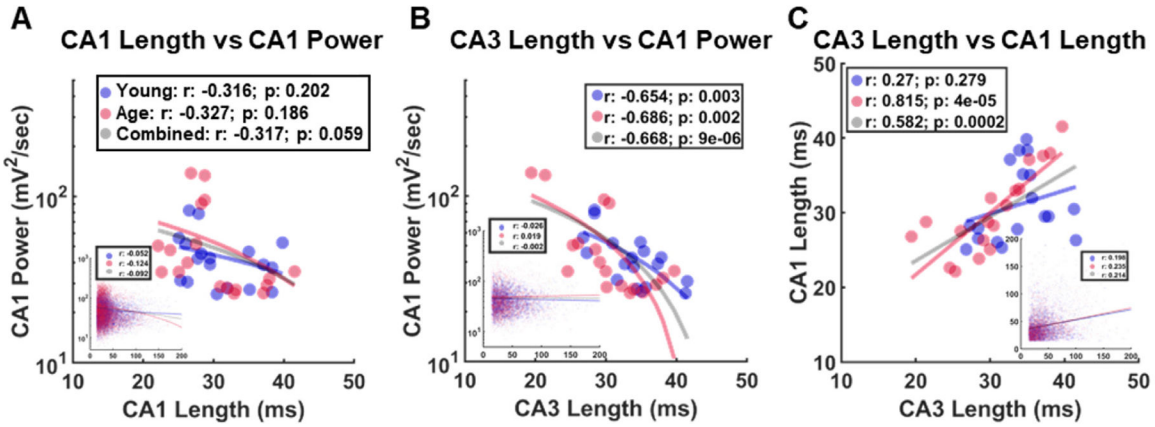

Fig. 6.

Event Metric Relationships: Metric relationships shown are those with a greater than 0.4 loading onto any component of the PCA (Table 2). Each data point indicates the median value for a young (blue) or aged (red) rat for the indicated metric for each day (two data points per rat). Insets show correlations for all events. Grey bars are linear regressions with the age groups combined. CA3 HFE frequency was excluded due to problematic loadings on to multiple components. **(A)** While CA1 ripple length and power had high loadings onto component 1 of the PCA, none of the metrics for the young, aged, or the two age groups combined showed a significant correlation. **(B)** Both young ($r_{[16]} = -0.654$, $p = 0.003$), aged ($r_{[16]} = -0.686$, $p = 0.002$), as well as the combined group ($r_{[34]} = -0.668$, $p = 9e\text{-}6$) showed significant, negative correlations between CA1 ripple power and CA3 HFE length, although this was not evident in the raw data. **(C)** CA1 ripple length was positively correlated with CA3 HFE length in aged rats ($r_{[16]} = 0.815$, $p = 4e\text{-}5$), but not in young animals ($r_{[16]} = 0.27$, $p = 0.279$), while the combined data was also significant ($r_{[34]} = 0.582$, $p = 0.0002$). "(For interpretation of the references to color in this figure legend, the reader is referred to the Web version of this article.)"

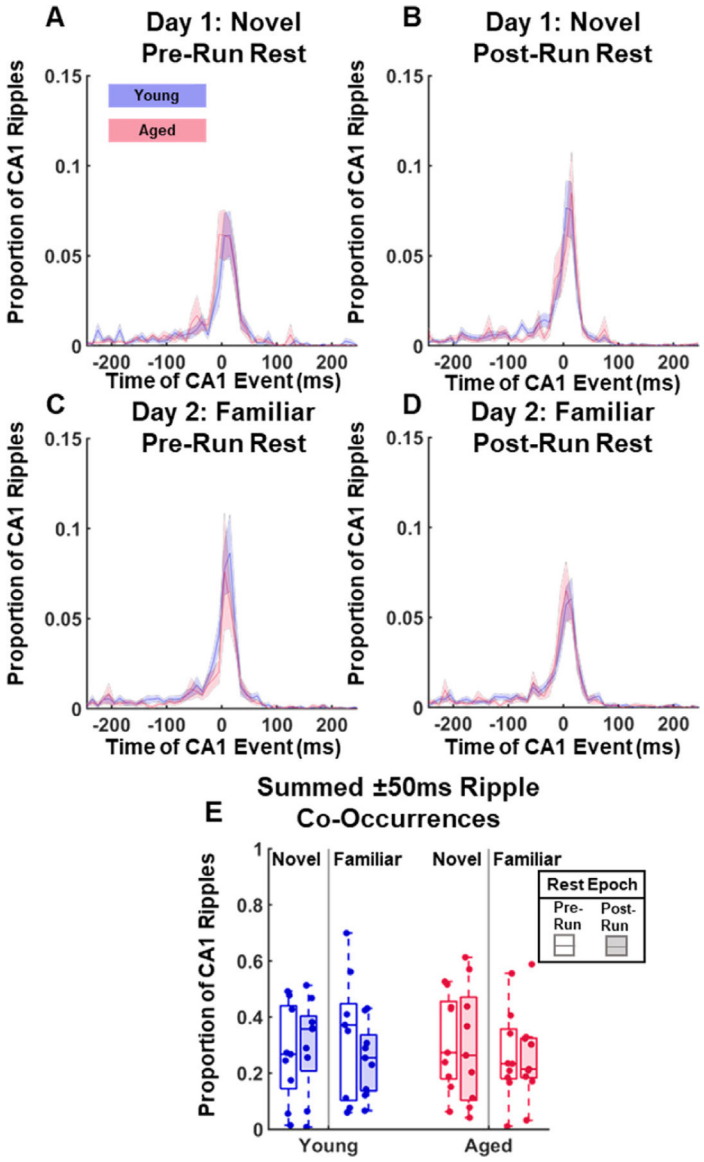

Fig. 7.

CA1 Ripple Co-Occurrence with CA3 HFEs by Day, Rest Epoch, and Age. (A–D) Average histograms (with standard error of the means) of the proportions of CA1 ripples that had a corresponding CA3 HFE. Ripple timing was measured from the peak power of the respective event. Global maximums tended to occur between±50 ms. **(E)** Significance was calculated based on the summed proportions between±50 ms with a Mixed Model ANOVA (between: Age and Familiarity; within: Rest Epoch). There were no significant main effects or interaction effects. “(For interpretation of the references to color in this figure legend, the reader is referred to the Web version of this article.)”

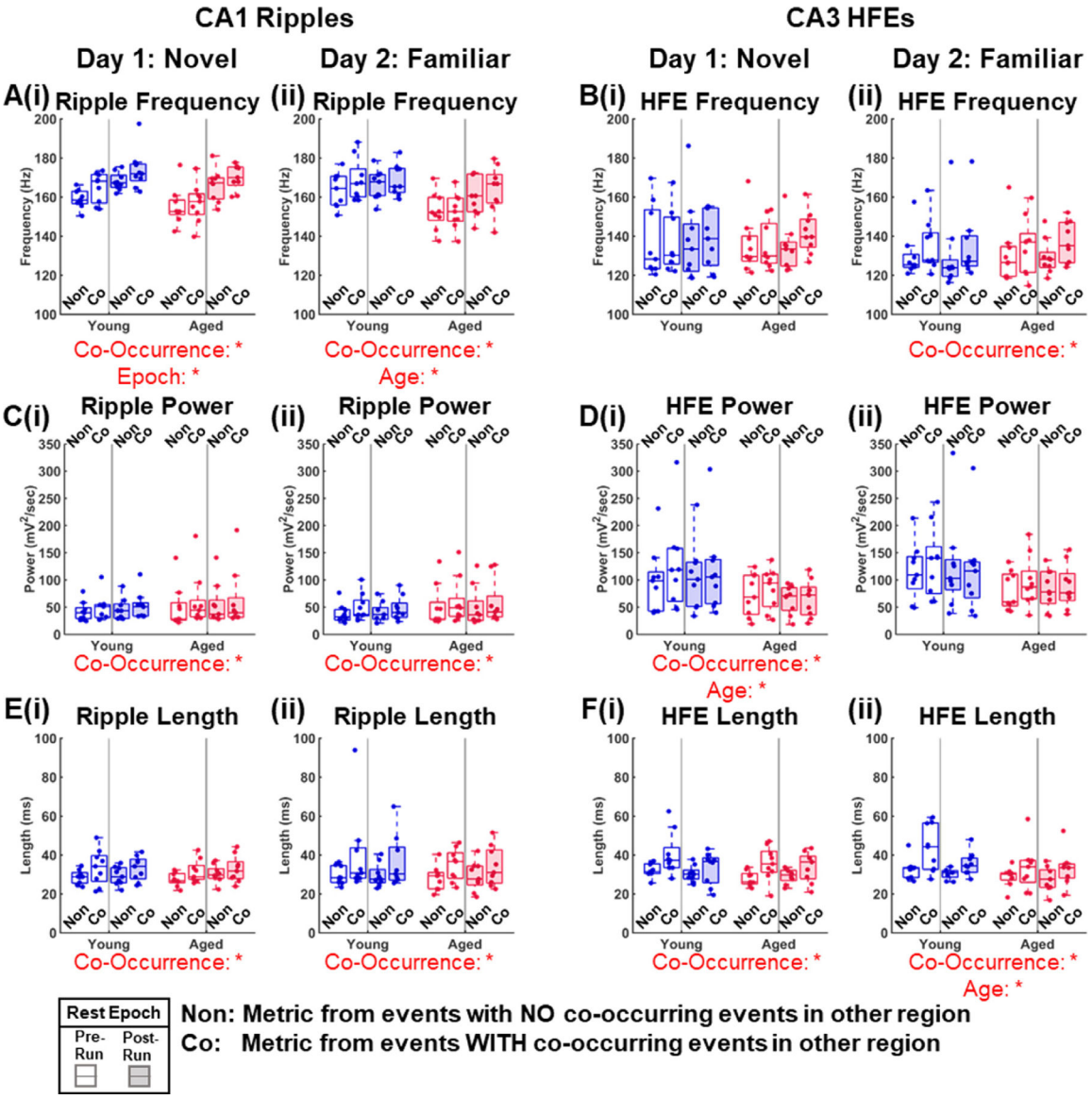

Fig. 8.

The co-occurrence of CA1 ripples and CA3 HFEs increased frequency, power, and length across age groups. CA1 ripple and CA3 HFE metrics were examined in relation to whether they co-occurred. Events that co-occurred with other events are labeled *(Co)*, and those that did not are labeled *(Non)*. Events were also separated by Day and pre/post run rest epoch. Across regions, age groups and days, frequency **(A/B)**, power **(C/D)**, length **(E/F)** values significantly increased between *Non* and *Co* ($F_{[1,32]}$ >7.2255, $p < 0.011$ for all comparisons), with the exceptions of CA3 Day 1 frequency **(Bi)** and Day 2 power **(Dii)**. There was a significant main effect of age for CA1 ripple frequency **(Aii)** ($F_{[1,32]} = 9.721$, $p = 0.0038$), CA3 HFE power **(Di)** ($F_{[1,32]} = 4.686$, $p = 0.038$), and CA3 HFE length **(Fii)** ($F_{[1,32]} = 4.791$, $p = 0.036$). The effect of rest epoch on CA1 ripple frequency was only significant the Day 1 **(Ai)** ($F_{[1,32]} = 18.834$, $p = 0.00013$). "(For interpretation of the references to color in this figure legend, the reader is referred to the Web version of this article.)"

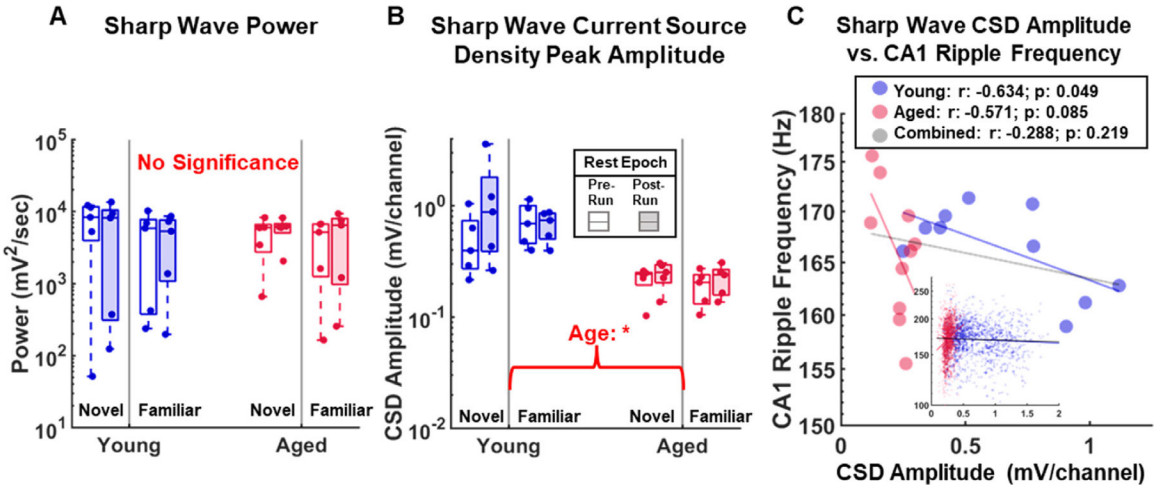

Fig. 9.

Stratum Radiatum Sharp Waves. Quantification of CA1 radiatum sharp waves and their relationship with CA1 ripple frequencies for Group 2 rats with linear probes spanning all hippocampal sub-layers ($N_{young} = 5$, $N_{age} = 5$). **(A)** Sharp wave power was not significant for either age, rest epoch, or familiarity ($F_{[1,16]} < 3.27$, $p > 0.089$ for all comparisons). **(B)** Sharp wave current source density (CSD) peak amplitude was significantly different across age groups ($F_{[1,16]} = 12.98$, $p = 0.0023$). **(C)** Correlation between sharp wave CSD peak amplitudes and CA1 ripple frequency. Data points for each epoch of each rat were included for a sample size of 10 per age group. Insets are the correlations for all ripples and sharp waves that co-occurred together (±50 ms) combined for all rats, days, and epochs. While the young rats had a p value of 0.049, this was not significant due to the Bonferroni correction made for multiple comparisons for a p-critical = 0.0166. “(For interpretation of the references to color in this figure legend, the reader is referred to the Web version of this article.)”

Table 1

Statistical results of event quantification metrics shown in figure 5.

Factor	CA1			CA3		
	Frequency	**Power**	**Length**	**Frequency**	**Power**	**Length**
Age	**F = 6.781 *p* = 0.014**	F = 1.07 *p* = 0.31	F = 0.0038 *p* = 0.95	F = 0.04 *p* = 0.82	**F = 4.16 *p* = 0.0498**	**F = 5.03 *p* = 0.032**
Day	F = 0.70 *p* = 0.41	F = 0.12 *p* = 0.73	F = 0.0064 *p* = 0.94	F = 0.78 *p* = 0.38	F = 0.42 *p* = 0.52	F = 0.0053 *p* = 0.94
Age x Day	F = 1.04 *p* = 0.32	F = 0.12 *p* = 0.91	F = 0.075 *p* = 0.79	F = 0.035 *p* = 0.85	F = 0.004 *p* = 0.95	F = 0.96 *p* = 0.33
Rest Epoch	**F = 70.053 *p* = 1.46e-9**	**F = 7.17 *p* = 0.01**	F = 2.49 *p* = 0.12	F = 0.39 *p* = 0.54	F = 0.15 *p* = 0.70	**F = 8.02 *p* = 0.0079**
Age x Epoch	**F = 7.84 *p* = 0.0086**	F = 1.58 *p* = 0.22	F = 2.88 *p* = 0.10	F = 0.049 *p* = 0.83	F = 0.18 *p* = 0.67	**F = 6.25 *p* = 0.018**
Day x Epoch	**F = 5.75 *p* = 0.023**	**F = 5.42 *p* = 0.026**	F = 3.13 *p* = 0.086	F = 1.487 *p* = 0.23	F = 1.10 *p* = 0.30	F = 1.303 *p* = 0.26
Age x Epoch	Epoch F = 0.88 *p* = 0.35	F = 0.78 *p* = 0.38	F = 0.14 *p* = 0.71	F = 0.005 *p* = 0.95	F = 0.87 *p* = 0.36	F = 0.017 p = 0.90

BOLD TYPE = significant (p<.05) All statistics are F[1,32], removed for readability

Table 2

Principal component analysis for CA1 and CA3 ripple metrics

Rotated Component Matrix([a])			
	Component		
	1	2	3
CA1 Frequency	0.05	0.001	0.982
CA3 Frequency	−0.667	−0.498	0.299
CA1 Power	−0.828	0.131	−0.291
CA3 Power	−0.077	0.97	0.032
CA1 Length	0.695	−0.056	−0.095
CA3 Length	0.895	0.076	0.07

Extraction Method: Principal Component Analysis

Rotation Method: Varimax with Kaiser Normalization

[a.] Rotation converged in 5 iterations.

Table 3

Statistical results for CA1 ripple metrics separated by co-occurrence with CA3 high frequency events.

Factor	Day 1			Day 2		
	Frequency	**Power**	**Length**	**Frequency**	**Power**	**Length**
Age	F = 3.38	F = 0.69	F = 0.16	**F = 9.72**	F = 1.01	F = 0.50
	p = 0.075	*p* = 0.41	*p* = 0.69	***p* = 0.004**	*p* = 0.32	*p* = 0.48
Rest Epoch	**F = 18.834**	F = 0.08	F = 0.35	F = 3.13	F = 0.004	F = 0.07
	***p* = 0.0001**	*p* = 0.77	*p* = 0.56	*p* = 0.086	*p* = 0.95	*p* = 0.80
Age x Rest Epoch	F = 0.45	F = 0.001	F = 0.34	F = 1.61	F = 0.008	F = 0.10
	p = 0.51	*p* = 0.97	*p* = 0.57	*p* = 0.21	*p* = 0.93	*p* = 0.76
Co-Occurrence	**F = 15.52**	**F = 15.26**	**F = 20.56**	**F = 7.25**	**F = 40.01**	**F = 17.13**
	***p* = 0.0004**	***p* = 0.0005**	***p* = 8e-5**	***p* = 0.011**	***p* = 4e-7**	***p* = 0.0002**
Age x Co-Occurrence	F = 1.90	F = 0.371	F = 0.52	F = 1.14	F = 0.12	F = 0.69
	p = 0.18	*p* = 0.55	*p* = 0.48	*p* = 0.29	*p* = 0.73	*p* = 0.41
Rest Epoch x Co-Occurrence	F = 0.21	F = 0.26	F = 0.72	F = 0.12	F = 1.10	F = 0.61
	p = 0.65	*p* = 0.61	*p* = 0.40	*p* = 0.73	*p* = 0.30	*p* = 0.44
Age x Rest Epoch x Co-Occurrence	F = 0.23	F = 0.14	F = 0.02	F = 1.93	F = 0.36	F = 0.10
	p = 0.63	*p* = 0.71	*p* = 0.89	*p* = 0.17	*p* = 0.56	*p* = 0.75

BOLD TYPE = significant ($p < 0.05$) All statistics are F[1,32], removed for readability

Table 4

Statistical Results for CA3 High Frequency Event Metrics Separated by Co-Occurrence with CA1 Ripple Events

Factor	Day 1			Day 2		
	Frequency	**Power**	**Length**	**Frequency**	**Power**	**Length**
Age	F = 0.031	**F = 4.69**	F = 1.48	F = 0.016	F = 3.63	**F = 4.79**
	p = 0.86	***p* = 0.038**	*p* = 0.23	*p* = 0.90	*p* = 0.066	***p* = 0.036**
Rest Epoch	F = 0.22	F = 0.17	F = 1.38	F = 0.001	F = 0.013	F = 1.96
	p = 0.64	*p* = 0.68	*p* = 0.25	*p* = 0.97	*p* = 0.91	*p* = 0.17
Age x Rest Epoch	F = 0.024	F = 0.087	F = 1.23	F = 0.008	F = 1.88e-5	F = 0.88
	p = 0.88	*p* = 0.77	*p* = 0.28	*p* = 0.93	*p* = 0.997	*p* = 0.35
Co-Occurrence	F = 1.53	**F = 11.02**	**F = 24.05**	**F = 17.41**	F = 2.76	**F = 24.66**
	p = 0.22	***p* = 0.0023**	***p* = 3e-5**	***p* = 0.0002**	*p* = 0.11	***p* = 2e-5**
Age x Co-Occurrence	F = 1.22	F = 2.74	F = 0.089	F = 0.065	F = 0.60	F = 1.25
	p = 0.28	*p* = 0.11	*p* = 0.77	*p* = 0.80	*p* = 0.45	*p* = 0.27
Rest Epoch x Co-Occurrence	F = 1.85	F = 3.51	F = 2.68	F = 0.37	F = 3.95	F = 0.88
	p = 0.18	*p* = 0.070	*p* = 0.11	*p* = 0.55	*p* = 0.055	*p* = 0.36
Age x Rest Epoch x Co-Occurrence	F = 1.12	F = 0.18	F = 0.19	F = 0.56	F = 0.50	F = 1.41
	p = 0.28	*p* = 0.67	*p* = 0.67	*p* = 0.46	*p* = 0.49	*p* = 0.24

BOLD TYPE = significant (p<.05) All statistics are F[1,32], removed for readability